Cenozoic shortening budget for the northeastern edge of the Tibetan Plateau: Is lower crustal flow necessary?

Richard O. Lease,[1,2] Douglas W. Burbank,[1] Huiping Zhang,[3] Jianhui Liu,[4] and Daoyang Yuan[5]

Received 15 November 2011; revised 1 April 2012; accepted 17 April 2012; published 30 May 2012.

[1] Two of the most popular mechanisms for thickening the crust beneath the Tibetan Plateau are (1) pure shear with faulting and folding in the upper crust and horizontal shortening below and (2) flow of lower or middle crust without significant shortening of the upper crust. To help discriminate between the relative contributions of these two mechanisms, well-constrained estimates of upper crustal shortening are needed. Here we document the Cenozoic shortening budget across the northeastern Tibetan Plateau margin with several balanced cross sections that exploit thermochronological and magnetostratigraphic constraints. These sections indicate 11 $^{+2}/_{-1}$% east-west shortening since middle Miocene time and ~9 $^{+2}/_{-3}$% NNE-SSW shortening between middle Eocene and middle Miocene times with little subsequent shortening of this orientation. Shortening rates accelerate fivefold after middle Miocene time. Given the present-day crustal thickness of 56 ± 4 km in northeastern Tibet, crustal restorations that remove Cenozoic shortening suggest that the northeastern Tibetan crust was 45 ± 5 km thick prior to the India-Asia continental collision. This precollision thickness estimate is equivalent to average continental crustal thicknesses both adjacent to the Tibetan Plateau (44 ± 4 km) and globally (41 ± 6 km) and suggests that pure shear alone may account for Cenozoic crustal thickening in northeastern Tibet. In contrast to eastern Tibet where, in the absence of significant shortening structures, crustal flow has been invoked to explain the addition of crustal material since middle Miocene time, our results may obviate lower crustal flow as a necessary crustal thickening agent in northeastern Tibet.

Citation: Lease, R. O., D. W. Burbank, H. Zhang, J. Liu, and D. Yuan (2012), Cenozoic shortening budget for the northeastern edge of the Tibetan Plateau: Is lower crustal flow necessary?, *Tectonics*, *31*, TC3011, doi:10.1029/2011TC003066.

1. Introduction

[2] Perhaps the most direct consequence of the collision of two buoyant continents is large-scale crustal thickening that results in the upward and outward growth of high terrain. As the stronger Indian continent has collided with weaker Asia over at least the past 50 Myr [*Beck et al.*, 1995; *Garzanti and Van Haver*, 1988; *Najman et al.*, 2010; *Zhu et al.*, 2005], widespread crustal thickening has occurred over an area that is approximately 2.5 million km^2 at present. The resultant Tibetan crust is the thickest observed on Earth today with an average thickness of 65 km and a maximum that may reach 90 km in places [*Kind et al.*, 2002; *Nabelek et al.*, 2009; *Owens and Zandt*, 1997; *Wittlinger et al.*, 2004; *Zhao et al.*, 2001]. The mechanisms by which Tibetan crust has thickened, however, as well as the timing and distribution of these mechanisms across the plateau, remain debatable.

[3] Thickening of the crustal column can reflect both ductile flow and inflation of the lower crust [e.g., *Bird*, 1991] in addition to brittle faulting and folding due to crustal shortening. Whereas ductile lower crustal flow is interpreted to have played a significant role in the Cenozoic thickening of eastern Tibetan crust starting in middle Miocene time (summarized in *Royden et al.* [2008]), brittle crustal shortening was dominant in northern Tibet and persistent throughout the Cenozoic era (Figure 1) [e.g., *Yin et al.*, 2008b]. In eastern Tibet ~500 km to the south of our study area, an influx of weak, low-viscosity, lower crustal material [e.g., *Clark and Royden*, 2000; *Royden et al.*, 1997] is interpreted to have passively thickened the crust in the absence of significant crustal shortening (Figure 1) [*Burchfiel et al.*, 1995; *King et al.*, 1997]. This crustal flow interpretation for eastern Tibet, however, is not without critics [e.g., *Hubbard and Shaw*, 2009; *Liu-Zeng*

[1]Department of Earth Science, University of California, Santa Barbara, California, USA.
[2]Now at U.S. Geological Survey, Anchorage, Alaska, USA.
[3]State Key Laboratory of Earthquake Dynamics, Institute of Geology, China Earthquake Administration, Beijing, China.
[4]Institute of Geology, Chinese Academy of Geological Sciences, Beijing, China.
[5]Lanzhou Institute of Seismology, China Earthquake Administration, Lanzhou, China.

Corresponding author: R. O. Lease, U.S. Geological Survey, 4200 University Dr., Anchorage, AK 99508, USA. (rlease@usgs.gov)

0278-7407/12/2011TC003066

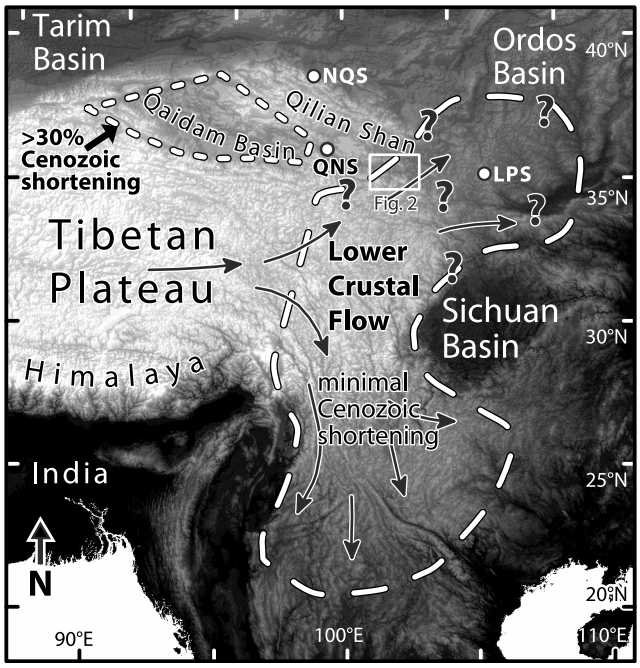

Figure 1. Eastern half of the Tibetan Plateau displaying inferred zone of late Cenozoic lower crustal flow in eastern Tibet [*Clark and Royden*, 2000; *Clark et al.*, 2005; *Klemperer*, 2006] and zone of >30% Cenozoic crustal shortening in Qilian Shan–Qaidam basin [*Yin et al.*, 2007, 2008a, 2008b]. The relative contribution of these two processes in thickening the northeastern margin of Tibet is unknown. Location of studies discussed in text: NQS, North Qilian Shan; QNS, Qinghai Nan Shan; LPS, Liupan Shan.

et al., 2008]. *Hubbard and Shaw* [2009] used balanced cross sections to infer that crustal shortening alone is sufficient to explain the crustal thickness of the Longmen Shan.

[4] In contrast, in northern Tibet across the Qaidam basin and the bounding Qilian Shan and Kunlun Shan ranges ~500 km to the west of our study area, several, serial, balanced cross sections display an average Cenozoic crustal shortening strain of >30% (Figure 1) [*Yin et al.*, 2007, 2008a, 2008b]. *Yin et al.* [2008a] interpret this crustal shortening to be solely responsible for generating the modern, ~50 km thick Qaidam crust [*Karplus et al.*, 2011; *Shi et al.*, 2009]. Geophysical data, on the other hand, have been interpreted to show localized, lower crustal injection beneath the southern Qaidam basin–Kunlun margin [*Karplus et al.*, 2011]. Between these two areas (i.e., eastern and northern Tibet) with purportedly contrasting crustal thickening mechanisms lies our study area in northeastern Tibet, where the relative importance of crustal shortening versus lower crustal flow as crustal thickening agents is unknown (Figure 1).

[5] The northeastern margin of the Tibetan Plateau centered at 36°N 102.5°E has a modern crustal thickness of 56 ± 4 km (Figure 2), based on receiver function analyses [*Pan and Niu*, 2011] and a seismic refraction profile [*Liu et al.*, 2006]. A similar 56 km thickness estimate is also from nearby seismic reflection profiles [*Galvé et al.*, 2002; *Jiang et al.*, 2006] and from inversions of regional gravity data [e.g., *Braitenberg et al.*, 2000]. How shortening and thickening have occurred in northeastern Tibet, however, remains debatable. *Clark and Royden* [2000] model the northeastward sloping topography across the northeastern Tibetan Plateau with an underlying 15 km thick lower crustal channel and interpret crustal flow in the corridor between the Qaidam and Sichuan basins that encompasses our study area (Figure 1) [*Clark and Royden*, 2000; *Clark et al.*, 2005]. *Pan and Niu* [2011], however, measure a very low Poisson's ratio (0.240) beneath the northeastern margin of the Tibetan Plateau and interpret a generally felsic crustal column that is inconsistent with lower crustal flow and addition of mafic lower crust. Furthermore, *Yin et al.* [2008a] document persistent crustal shortening throughout the Cenozoic a few hundred kilometers to the west of this inferred flow corridor. Finally, *Klemperer* [2006] reviewed geophysical data and interpreted no lower crustal flow in the Qaidam lower crust, but eastward lower crustal flow in the area north of Sichuan basin.

[6] A first step toward assessing the mechanisms by which northeastern Tibetan crust became thickened is determining the magnitude, timing, and rates of upper crustal shortening through geological mapping and cross section construction. In this contribution, we present two sets of cross sections that traverse the margin of the plateau near 36°N 102.5°E and span 145 by 100 km. Our cross sections exploit chronological constraints from thermochronology of bounding ranges [*Clark et al.*, 2010; *Lease et al.*, 2011] and magnetostratigraphy of adjacent basin fills [*Fang et al.*, 2003, 2005; *Hough et al.*, 2011; *Lease et al.*, 2012]. Balanced reconstructions of the cross sections indicate ~11 $^{+2}/_{-1}$% east-west shortening since middle Miocene time and ~9 $^{+2}/_{-3}$% NNE-SSW shortening since middle Eocene time.

2. Geological Setting

[7] The south Qilian Shan suture zone, which coincides with the position of the northern boundary of the Triassic Kunlun arc [*Yin and Harrison*, 2000], is a prominent feature in our study area and separates Permo-Triassic flysch and plutonic rocks in the south from early Paleozoic sedimentary and plutonic rocks in the north (Figure 2) [*QBGMR*, 1991]. Reactivation of this suture zone in middle Eocene time is documented by the onset of rapid cooling on the hanging wall of the NNE vergent West Qinling reverse fault (Figure 2) [*Clark et al.*, 2010; *Duvall et al.*, 2011]. The Eocene initiation of NNE-SSW contraction on the northeastern plateau margin [*Clark et al.*, 2010; *Yin et al.*, 2002, 2008a] was coincident with initial India-Asia continental collision occurring >3000 km to the south [*Molnar and Stock*, 2009].

[8] NNE-SSW contraction continued in northeastern Tibet for several tens of Myr as suggested by the early Miocene onset of motion on the Laji Shan reverse fault ~60 km to the north of the West Qinling (Figure 2) [*Lease et al.*, 2011]. In this paper, we quantify shortening across both of these NNE vergent structures. By middle Miocene time, however, new structures accommodating east-west shortening of this region of Tibet initiated. The start of rapid cooling on the

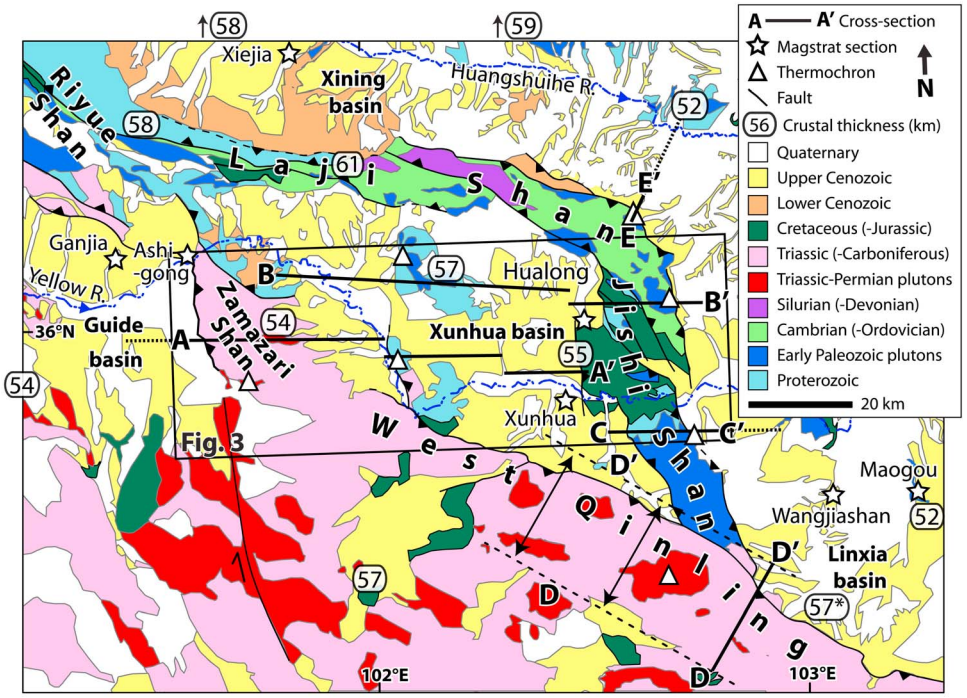

Figure 2. Geological overview map of study area. See Figure 1 for location. Displayed are locations of strip map (Figure 3) and cross sections, low-temperature thermochronological samples, and age-elevation transects (triangles) [this study, *Clark et al.*, 2010; *Lease et al.*, 2011], magnetostratigraphic sections (stars) [*Dai et al.*, 2006; *Fang et al.*, 2003, 2005; *Hough et al.*, 2011; *Lease et al.*, 2012], and crustal thickness measurements based on receiver functions [*Pan and Niu*, 2011] except for one measurement from a seismic refraction survey (denoted with an asterisk) [*Liu et al.*, 2006]. Dotted lines west of A, north of E′, and east of C′ reflect undeformed cross-sectional lengths added to composite cross sections when determining regional shortening—see sections 4.4 and 5.3 for rationale.

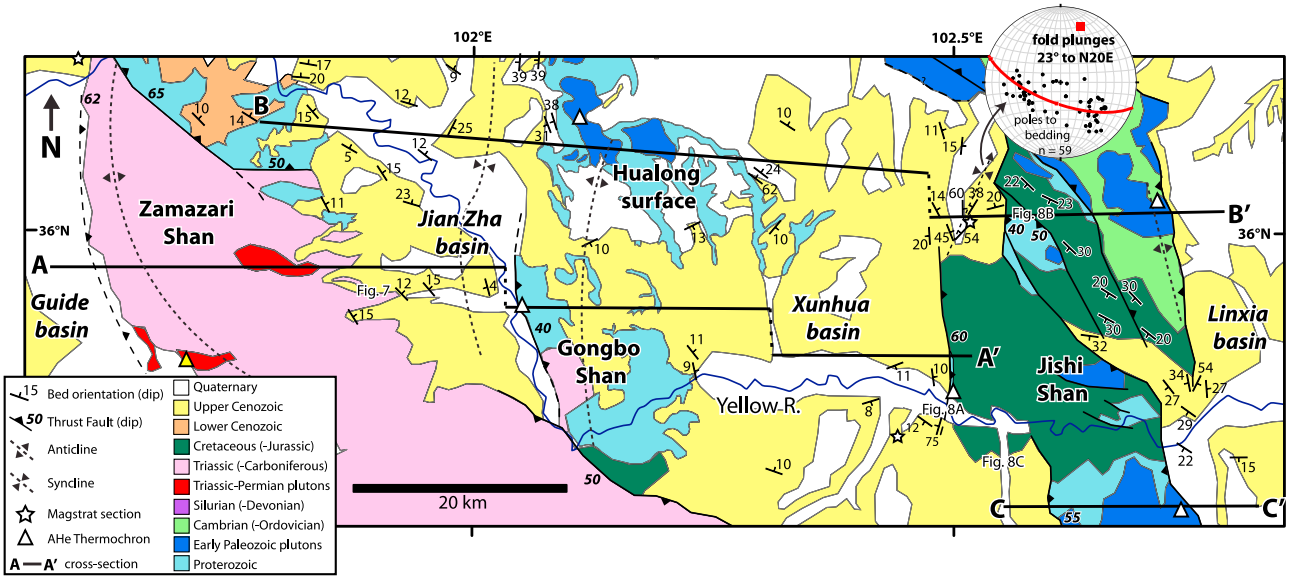

Figure 3. Geological map of the northeastern Tibetan Plateau showing representative bedding orientation measurements of Cenozoic and Cretaceous strata and major Cenozoic structures. See Figure 2 for location. Cross sections are displayed in Figures 4–6. Locations of Figures 7 and 8 field photos noted. The yellow triangle denotes new thermochronology sample presented in this paper; white triangles denote samples reported in *Lease et al.* [2011]. Geology modified after *QBGMR* [1991] and *GBGMR* [1991] with our own measurements and interpretations.

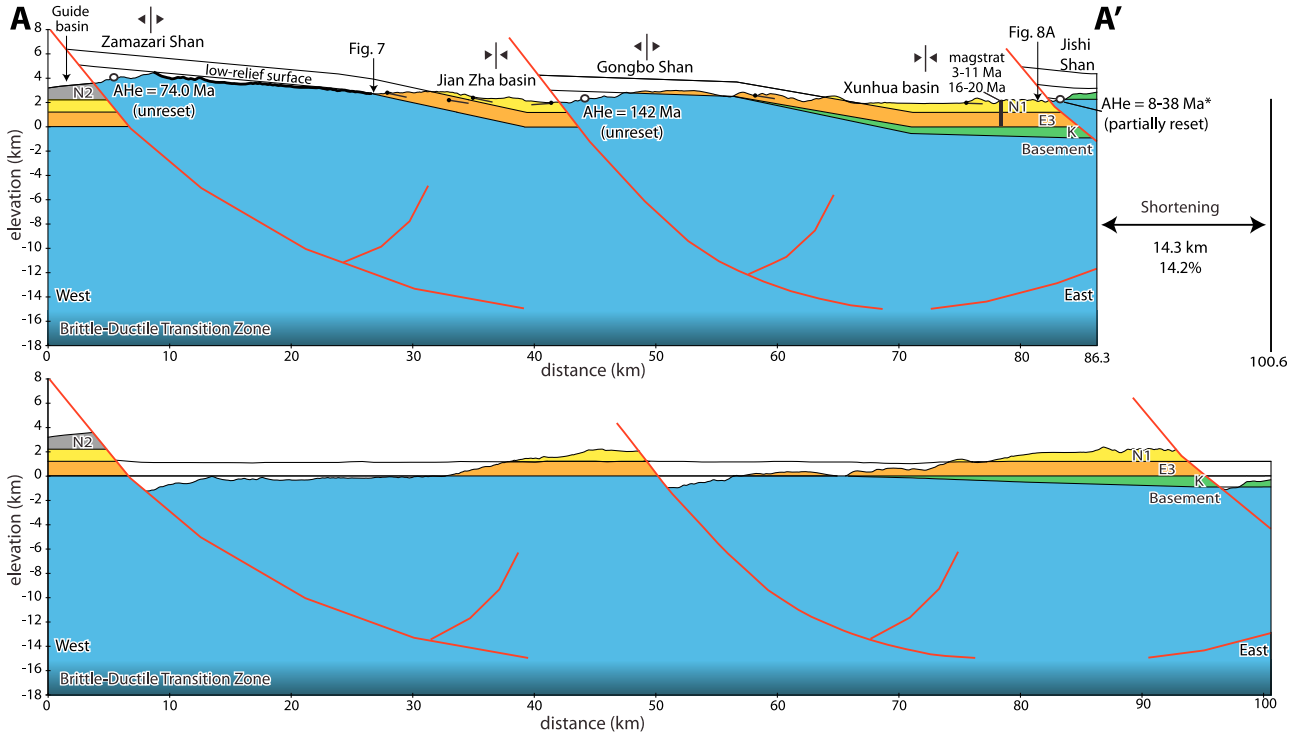

Figure 4. East-west cross section A–A′. Apatite (U-Th)/He ages from this study and *Lease et al.* [2011] and southern Xunhua basin magnetostratigraphic section from *Hough et al.* [2011]. See Figure 3 for location. The structural geology of this area is dominated by reverse fault-bounded ranges spaced at ~40 km intervals. The long 15–38 km wavelength of gentle back-tilting on the hanging wall combined with a modest 4–8 km displacement on any given fault suggests that faults become listric with depth.

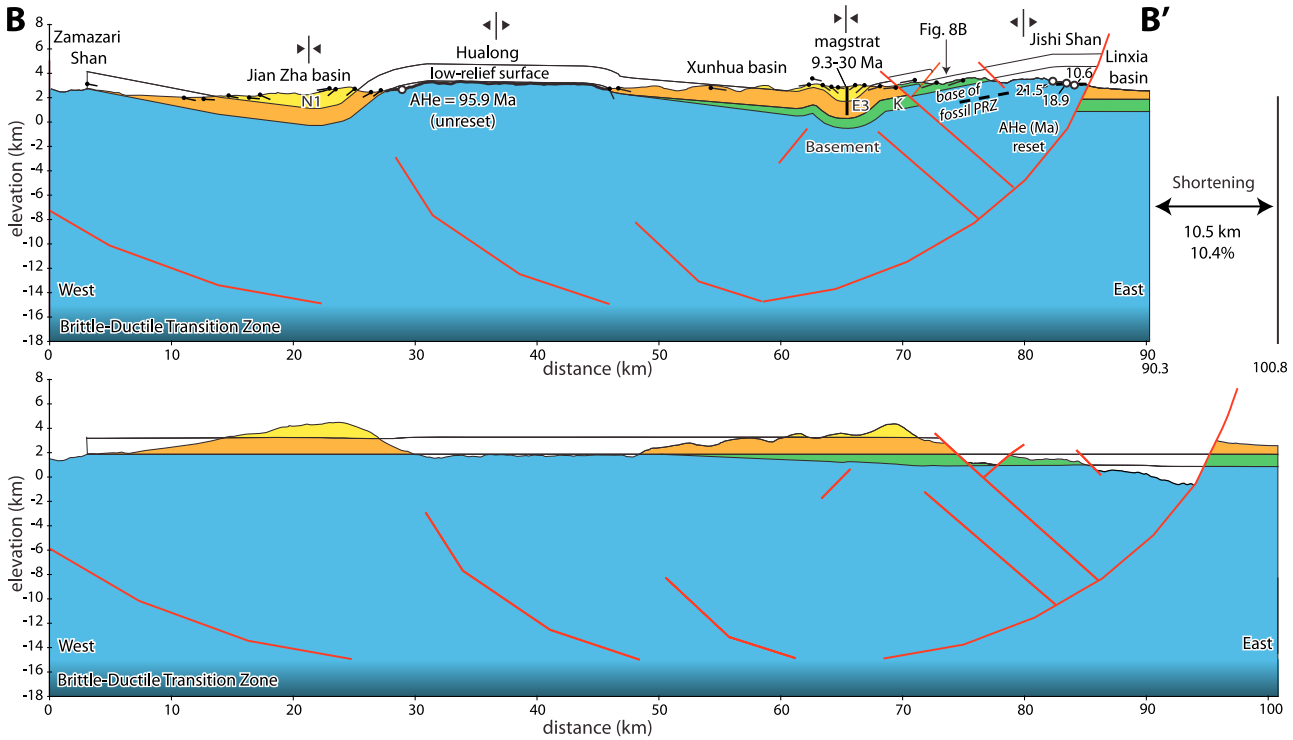

Figure 5. East-west cross section B–B′. Apatite (U-Th)/He ages from *Lease et al.* [2011] and northern Xunhua basin magnetostratigraphic section from *Lease et al.* [2012]. See Figure 3 for location.

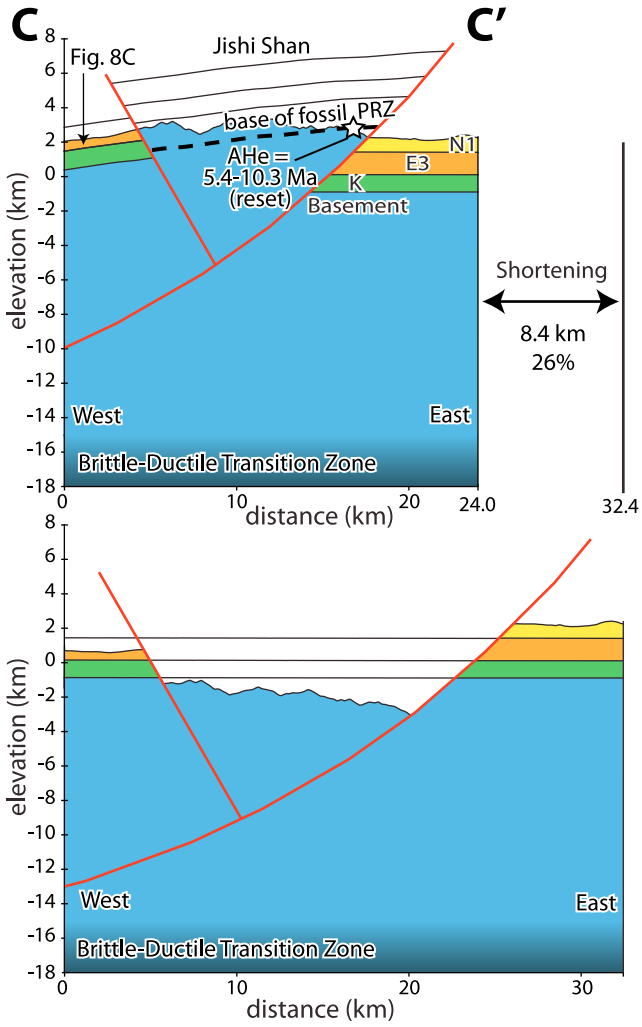

Figure 6. East-west cross section C–C′. Apatite (U-Th)/He ages are from *Lease et al.* [2011]. See Figure 3 for location.

hanging walls of the east vergent Jishi Shan [*Lease et al.*, 2011] and Liupan Shan [*Zheng et al.*, 2006] reverse faults at ~13 and 8 Ma, respectively, highlights the commencement of east-west shortening over a corridor that extends 320 km to the east of the Jishi Shan. In this paper, we quantify the magnitude of shortening across the Jishi Shan and subsidiary west vergent ranges that are located in a 145 km long corridor to the west of the Jishi Shan (Figure 2).

[9] These new structures accommodating east-west contraction were active contemporaneously with the late Miocene initiation of structures nearby that continued to accommodate NNE-SSW contraction, e.g., the North Qilian Shan fault [*Bovet et al.*, 2009; *Zheng et al.*, 2010] and Qinghai Nan Shan fault (Figure 1) [*Zhang et al.*, 2012]. The concurrent slip on these two sets of faults of contrasting orientation may signal the start of the modern tectonic regime in northeastern Tibet where contraction is coupled to strike-slip faulting in a regional stepover [*Duvall and Clark*, 2010].

[10] Northeastern Tibet contains a rather complete Cenozoic sedimentary succession with continuous fluvial and/or lacustrine deposition from 52 to 2 Ma. Magnetostratigraphy indicates that the base of the Cenozoic fill is ~52 Ma in Xining basin [*Dai et al.*, 2006], and >30 Ma in Xunhua and Linxia basins to the south [*Fang et al.*, 2003; *Lease et al.*, 2012]. A 25° clockwise rotation in the Paleogene basin system that occurred in Eocene time [*Dupont-Nivet et al.*, 2008] corroborates early collision-related deformation. In Miocene time, on the other hand, depositional episodes characterized by accelerated sediment accumulation, as well as the introduction of new sources [*Lease et al.*, 2007], reflect punctuated erosion of mountain ranges [*Lease et al.*, 2012] that overall suggest a kinematic shift with the onset of east-west shortening [*Lease et al.*, 2011]. Finally, a transition from basin filling to excavation began at ~1.8 Ma as Yellow River incision commenced on the plateau margin

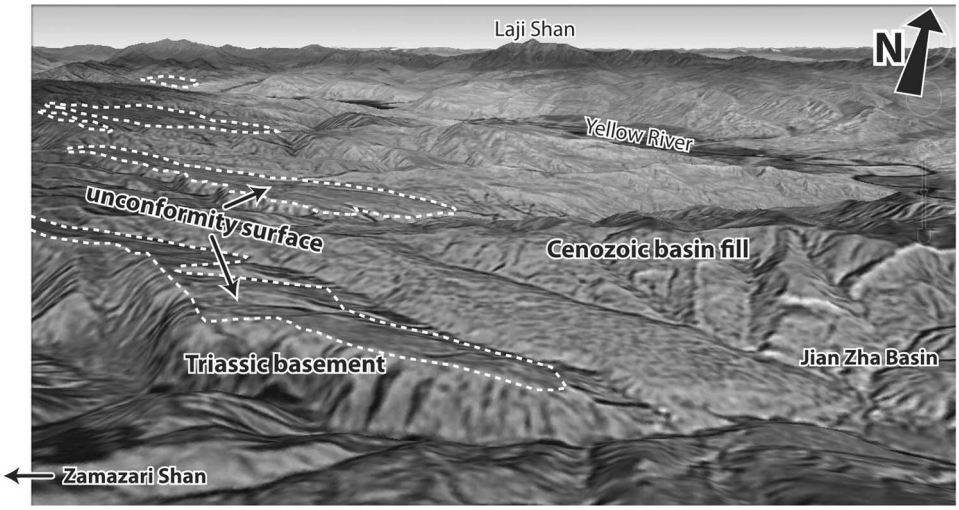

Figure 7. Widespread low-relief exhumed unconformity surface between the base of the Cenozoic cover strata and the underlying erosionally resistant basement. We use the surface as a strain marker, i.e., to measure displacement across faults where late Cenozoic strata are absent. Oblique view from along the western side of Jian Zha basin/eastern flank of Zamazari Shan Range (location shown in Figures 3 and 4). Image modified from Google Earth.

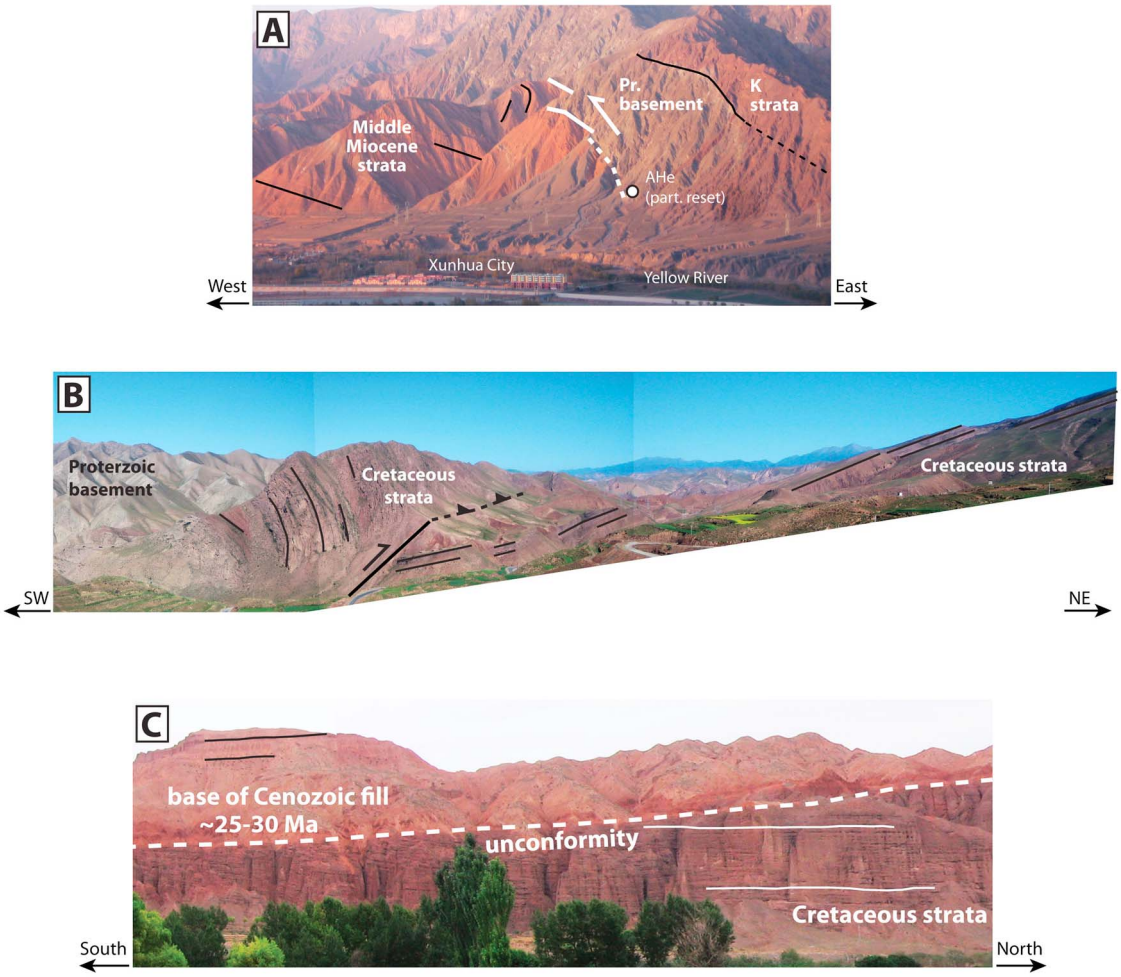

Figure 8. Key field observations. Photo locations shown in Figure 3 map and cross section Figures 4–6. (a) Example of basement-Cenozoic cover faulting relationships in this area. Footwall strata commonly show short-wavelength drag folding. Photo of Jishi Shan back thrust with footwall ages constrained from southern Xunhua basin magnetostratigraphy [*Hough et al.*, 2011]. Apatite (U-Th)/He age from the hanging wall was partially reset in Cenozoic time and contained replicate ages of 8, 19, and 39 Ma from which no representative mean age was calculated [*Lease et al.*, 2011]. (b) Example (on right half of image) of several-kilometer-long homocline of moderately dipping Cretaceous strata that we utilize to constrain fault geometry at depth. Example (on left side of image) of basement-cored reverse fault with short-wavelength folding of Cretaceous strata on hanging wall. (c) Example of Cretaceous-Cenozoic unconformity typical of many parts of our study area. Given the <5° angular discordance between the Cretaceous and Cenozoic strata, we assert that deformation of the Cretaceous unit records principally Cenozoic deformation.

and progressed upstream [*Craddock et al.*, 2010; *Harkins et al.*, 2007].

3. Methods

[11] We conducted reconnaissance field mapping (Figure 3) with the goal of constructing a series of east-west cross sections that characterized the style and magnitude of Cenozoic deformation. Our mapping expanded upon previous geological maps of this area [*Gansu Provincial Bureau of Geology and Mineral Resources* (*GBGMR*), 1991; *Qinghai Provincial Bureau of Geology and Mineral Resources* (*QBGMR*), 1991], and we constructed balanced cross sections (Figures 4–6) based on our measurements and observations in the field (Figures 7 and 8). Our east-west cross sections span a net across-strike distance of about 115 km and are aligned approximately along the 36°N parallel west of 103°E. Wherever feasible, the cross sections are tied directly to recently published thermochronological [*Lease et al.*, 2011] and magnetostratigraphic [*Fang et al.*, 2003, 2005; *Hough et al.*, 2011; *Lease et al.*, 2012] constraints on the timing of deformation and thickness of Cenozoic basin fill across this area. We restore our east-west cross sections to a predeformation state through line-length balancing [*Dahlstrom*, 1969] using the 2-D MOVE software package from Midland Valley.

[12] We present one new bedrock apatite (U-Th)/He age (AHe) from the Zamazari Shan on the western end of our east-west transect (Table 1 and Figure 4). We refer readers to *Clark et al.* [2010] and *Lease et al.* [2011] for a description

Table 1. Apatite (U-Th)/He Data[a]

	U (ppm)	Th (ppm)	He (nmol/g)	Mass (μg)	Ft[b]	Radius (μm)	Length (μm)	Raw Age (Ma)	Corrected Age (Ma)
Sample ZS6-A(a)	8.1	34	3.9	1.0	0.62	36	142	44.3	72.0
Sample ZS6-A(b)	15	43	6.7	1.3	0.63	35	198	49.5	78.2
Sample ZS6-A(c)	6.5	27	3.2	1.1	0.62	36	163	45.1	72.3
Sample ZS6-A(d)	13	31	5.9	3.7	0.74	53	240	54.3	73.2
Average									73.9

[a]Sample location: 35.893°N, 101.697°E, 3461 m elevation. Data consist of four single-grain analyses.
[b]FT is alpha-ejection correction after *Farley et al.* [1996].

of analytical methods. With a nominal closure temperature of 60–70°C [*Flowers et al.*, 2009], (U-Th)/He dating of apatite dates cooling in the upper crust as rocks come within 2–4 km depth of the surface. In thrust belts, young or reset AHe ages commonly reflect accelerated cooling and erosion of rocks in response to accelerated thrust or reverse faulting.

[13] To estimate the magnitude of NNE-SSW shortening, we constructed cross sections across the two principal NNE vergent reverse structures in this area, the West Qinling and Laji Shan faults (Figures 9 and 10). Thermochronology age-elevation transects delimit the timing and magnitude of Cenozoic rock cooling associated with erosion of reverse fault hanging walls concurrent with fault displacement [*Clark et al.*, 2010; *Lease et al.*, 2011]. Magnetostratigraphy constrains the chronology and thickness of the footwall strata, as well as helps infer these parameters for the now eroded, hanging wall strata [*Dai et al.*, 2006; *Fang et al.*, 2003; *Hough et al.*, 2011; *Lease et al.*, 2012].

4. Results for East-West Cross Sections

4.1. Observations

[14] The geology of our study area is dominated by ranges that are spaced at ~40 km intervals and are bounded by reverse faults (Figures 4–6). From east to west, these ranges are the Jishi Shan, Gongbo Shan, and Zamazari Shan (Figures 3 and 4). Intervening basins preserve an up to 2–3 km thickness of Cenozoic fill. Fault dips measured at the surface are relatively steep, measuring 40–65° (Figure 3 and our measurements) [*GBGMR*, 1991; *QBGMR*, 1991]. In addition, large-scale field observations (Figure 8) suggest steeply dipping faults. We assume pure dip-slip across faults and acknowledge that this assumption of plane strain introduces uncertainty in our shortening estimates (see section 6.3, second paragraph). Unfortunately, we did not discover fault striations during our field investigations that would have more confidently delimited fault slip, and hence, shortening directions.

[15] We define five structural units in our cross sections. The undifferentiated basement unit, where exposed, is composed variably of Proterozoic, Paleozoic, and Triassic igneous, sedimentary, and metamorphic rocks (Figure 2) [*GBGMR*, 1991; *QBGMR*, 1991]. Overlying the basement locally is a Cretaceous unit of fluviolacustrine strata. This unit is up to 1 km in thickness at the eastern end of our sections [*Horton et al.*, 2004]. We document a minor angular unconformity between the Cretaceous and Cenozoic units in this area that is commonly <5° (Figure 8c). Cenozoic units E3, N1, and N2 (Figure 4) are generally Oligocene, early-middle Miocene, and late Miocene–Pliocene in age, respectively. We define unit E3 as starting at the base of the Cenozoic basin fill, which is documented in northern Xunhua basin and Linxia basin to be >30 Ma [*Fang et al.*, 2003; *Hough et al.*, 2011; *Lease et al.*, 2012]. The boundary between E3 and N1 is at approximately 20 Ma, and between N1 and N2, the boundary lies at ~9–13 Ma. Upper Neogene deposition (N2) continues until ~2 Ma: the top of the basin fill in this area [*Fang et al.*, 2003, 2005]. The presence of a widespread, low-relief, exhumed unconformity surface between the base of the cover strata (Unit E3) and the underlying, erosionally resistant basement provides a useful horizon that we use to measure displacement across faults

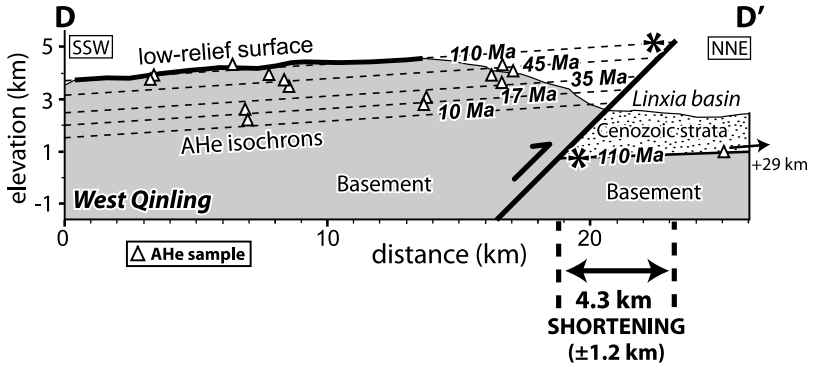

Figure 9. Cross section across the West Qinling reverse fault. Apatite (U-Th)/He data and figure modified from *Clark et al.* [2010]. Restoration of low-relief exhumed unconformity surface on the hanging wall with equivalent basement-cover unconformity on the footwall suggests 4.3 km of shortening across the fault since middle Eocene time. Correlative ~110 Ma AHe cooling ages on both hanging wall and footwall unconformity suggest a once-continuous surface that was later offset by faulting.

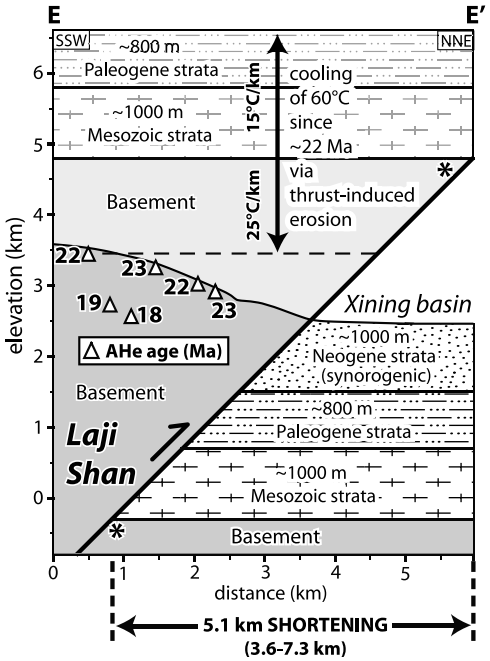

Figure 10. Cross section across the Laji Shan reverse fault. Thermochronology indicates erosion of overlying hanging wall rock equivalent to 60° of cooling starting at ~22 Ma [*Lease et al.*, 2011]. Magnetostratigraphy constrains thicknesses of Mesozoic and Cenozoic strata on both hanging wall and footwall [*Dai et al.*, 2006; *Fang et al.*, 2005; *Horton et al.*, 2004; *Lease et al.*, 2012]. Restoration of basement-cover unconformity across the fault suggests ~5.1 km of early Miocene shortening.

where late Cenozoic strata are absent (Figure 7). The unconformity surface defines the eastern slope of the Zamazari Shan, as well as the low-relief Gongbo Shan–Hualong surface (Figures 4 and 5). An unconformity surface of similar character has been documented in the Kyrgyz Tien Shan [*Burbank et al.*, 1999; *Oskin and Burbank*, 2007].

4.2. Structural Interpretations

[16] We use the measured fault offsets and the observed patterns of backlimb tilting to constrain the subsurface fault geometries. We interpret the prominent, range-bounding reverse faults to become listric in geometry with increasing depth [*Amos et al.*, 2007; *Erslev*, 1986; *Seeber and Sorlien*, 2000] for two principal reasons. First, we observe that the 4–8 km displacements across the reverse faults are much smaller than the 15–38 km lengths of the gently dipping backlimbs on the hanging wall of the same faults (Figures 4–6, 8b). This relatively long extent of backlimb tilting is most readily explained by a fault whose dip becomes gentler with increasing depth and contains multiple, minor axial surfaces. Second, a simple fault-bend folding model [*Suppe*, 1983] with a single ramp-flat transition is inconsistent with our observations. The fault-bend folding model predicts that the backlimb length should approximate the fault displacement [*Suppe*, 1983], whereas for the faults that we studied the backlimb lengths are 3–6 times greater than the displacements. Finally, we note that cross section restorations based on the steep fault dips measured at the surface give a conservative estimate of shortening: the primary quantity we seek to constrain in this study.

[17] We interpret secondary back thrusts [*McClay and Buchanan*, 1992] splaying from the primary reverse fault planes to account for backlimb deformation. The back thrust for the Jishi Shan breaks the surface and has up to 3 km of displacement (Figures 4–6, 8a). In the Gongbo Shan and Zamazari Shan, however, the back thrusts remain blind and develop fault-related folds at their tips, which are modeled as trishear fault propagation folds [*Erslev*, 1991] with only a few hundred meters of displacement (Figure 4). Although we interpret the folds in cross section B–B′ across the Hualong surface and Xunhua basin to be trishear fault propagation folds, multiple geometries of underlying faults could produce the folding observed at the surface. Regardless of structural interpretation, restoration of the base of the Cenozoic basin fill across folds and faults with measured dips (Figure 3) provides an estimate of minimum shortening across this section.

[18] We interpret the range-bounding reverse faults to sole into the brittle-ductile transition zone at 15 km depth below sea level (17–19 km depth below the surface). Both geometric constraints, as well as seismic data, justify such a deep zone. The long, 15–38 km extent of gentle backlimb tilting that we observe (Figure 4) requires a listric fault segment with a similar horizontal length. Simple geometric constraints indicate that a listric fault that dips 60° at the surface, has had 6 km of slip, and has a gentle 10° backlimb extending over a width of 38 km (e.g., Zamazari Shan fault; Figure 4) should extend to a depth of 17 km before linking with a planar fault [*Amos et al.*, 2007] (assuming rigid rotation along an arc). We choose a planar fault/transition zone depth of ~18 km below the surface as a preferred fit to the three primary reverse faults depicted in our cross sections (Figures 4–6). The 1990 Gonghe *Ms* ~ 6.9 earthquake near 36°N 100°E provides a glimpse into the structure of crustal faulting in this area of Tibet. Inversions of both leveling lines and waveforms agree that this large reverse slip event occurred on a steeply dipping (45–68°) fault with zones of concentrated slip extending to 14–16 km depth [*Chen et al.*, 1996].

4.3. Cross Section Construction

[19] We constructed our east-west cross sections (Figures 4–6) guided by the following six observations/data sets: (1) sedimentary thicknesses (1–3 km) are estimated from measured magnetostratigraphic sections [*Fang et al.*, 2003, 2005; *Hough et al.*, 2011; *Lease et al.*, 2012] and are assumed to be laterally uniform except where constrained by outcrop patterns (or other measured sections); (2) apatite (U-Th)/He thermochronology (AHe) [*Lease et al.*, 2011] provides thermal constraints for hanging wall erosion; (3) observed fault dips are steep (40–65°) [*GBGMR*, 1991; *QBGMR*, 1991]; (4) hanging walls have long, gently dipping backlimbs with lengths that greatly exceed fault displacement; (5) hanging wall cutoffs are preserved and defined by stratigraphic, geomorphic, and thermochronological data; and (6) hanging walls lack long forelimbs that dip into the faults (e.g., Figure 8a). Where beds are observed in contact with faults (Figure 8a), the absence of forelimbs suggests that the basement-cover unconformity can be reliably projected to the fault as a plane.

[20] A noteworthy asset of our cross sections is that they constrain both maximum and minimum allowable shortening, due to our ability to confidently reconstruct the hanging wall cutoffs of the pre-Oligocene unconformity. This asset contrasts with many structural studies where estimated shortening is solely a minimum, because hanging wall cutoffs are not preserved. Both magnetostratigraphy of cover strata and thermochronology of the underlying basement provide constraints on the timing and magnitude of burial, as well as exhumation, of the unconformity between these units.

[21] Mesozoic AHe ages from the hanging walls of many reverse faults in our study area indicate that Cenozoic burial reheating of the basement bedrock exposed at the surface today did not exceed ~70°C, the temperature at the base of the AHe partial retention zone [*Reiners and Brandon*, 2006]. Thus, Mesozoic AHe ages indicate that less than 2.8–3.6 km of rock overlying the samples was eroded in Cenozoic time assuming (1) near-surface geothermal gradients of 15°C/km for sedimentary rock and 25°C/km for basement rock [*Ehlers*, 2005; *Hu et al.*, 2000]; (2) known 1–3 km thicknesses of the Cenozoic sedimentary cover; and (3) 10°C mean annual surface temperature. Knowledge of the maximum allowed erosion constrains the position of the hanging wall cutoffs and thus places limits on maximum fault offset. On the footwalls directly beneath the reverse faults, we estimate uncertainties in the depth to the basement-cover unconformity to be ±500 m.

[22] Where our cross section crosses the Gongbo Shan, we utilize the basement-strata unconformity to measure displacement (~4 km) across the reverse fault that dips to the east below the range (Figure 4). Along strike of the Gongbo Shan to the north, this unconformity is expressed as an extensive low-relief surface, the "Hualong surface," which serves as a strain marker across a broad anticline in our northern cross section B–B′ (Figure 5). Mesozoic AHe ages of 142 and 96 Ma from low structural positions along the western edge of the Gongbo and Hualong surfaces, respectively (Figures 4 and 5), bound the maximum allowed erosion of this surface. We interpret 3 km of throw (i.e., vertical offset) across the Gongbo Shan reverse fault with a 2.5–3.8 km range of allowable throw given thermochronological and magnetostratigraphic constraints.

[23] On the eastern side of the Zamazari Shan at low elevations, the exhumed unconformity separating the basement from Cenozoic strata is exposed clearly for ~20 km as a near-planar surface (Figures 4 and 7). We project this surface across the Zamazari Shan crest to the projected reverse fault. The position of this unconformity surface, together with magnetostratigraphy [*Fang et al.*, 2005] and a Mesozoic AHe age of 74.0 Ma on the western side of the range, indicates a 4.5–5.8 km range of allowable throw and a preferred throw of 5 km.

[24] In the Jishi Shan, reverse faults on either side of the range dip in opposite directions (Figure 6). Two key observations lead us to interpret the Jishi Shan to be dominantly an east vergent reverse fault with a subsidiary west vergent back thrust. First, in the northern part of the range, Cretaceous strata define a >10 km long west dipping homocline with deeper structural levels exposed on the eastern side of the range. Given the only minor angular discordance between the Cretaceous and Cenozoic units (Figure 8c), we interpret the tilting of the Cretaceous unit to record primarily Miocene deformation. Second, in the southern part of the range where strata have not been preserved on top of the range, apatite fission track (AFT) cooling ages from the eastern flank of the age are notably younger (AFT 14–40 Ma) [*Lease et al.*, 2011] than those reported for the western flank (AFT 60–130 Ma) [*Dupont-Nivet et al.*, 2007] and, therefore, suggest a greater magnitude of exhumation (and, hence, reverse displacement) on the east.

[25] Across our composite, 115 km long, east-west cross section, Miocene AHe ages have been measured only for samples from the Jishi Shan and indicate that this range has experienced the greatest magnitude of late Cenozoic exhumation and, hence, reverse displacement (Figures 5 and 6). A detailed thermochronologic study of the eastern side of the Jishi Shan reveals the base of a fossil partial retention zone at ~3000 m elevation that marks a transition to rapid cooling of the range beginning at ~13 Ma [*Lease et al.*, 2011]. To aid in reconstructing shortening across the range, we use the elevation of this fossil partial retention zone to project the position of the base of the (now eroded) Cenozoic basin fill (Figures 5 and 6). We interpret 5.75 km of throw across the Jishi Shan reverse fault with uncertainties of ±0.5 km based on thermochronological and magnetostratigraphic constraints.

4.4. East-West Restorations

[26] In all of our cross-section reconstructions, we restored the base of the Cenozoic sedimentary strata (base of Unit E3) to horizontal. First, we restored displacement on secondary faults (e.g., back thrusts) that break the surface using the "fault-parallel flow" routine in the MOVE software package. Second, we restored displacement on the primary surface-breaking, range-bounding reverse faults using the same routine. Third, we explored blind fault geometries and trishear parameters [*Erslev*, 1991] that could produce the folding observed at the surface. We note that the blind faults presented in Figures 4, 5, and 6 are nonunique because this kinematic geometry is underconstrained. Fourth, we restored folds to horizontal using the "flexural slip" routine in MOVE.

[27] Line-length restoration of our cross sections provides an estimate of east-west horizontal shortening across the northeastern margin of the Tibetan Plateau. To determine net across-strike shortening in this area, we combine cross sections A–A′ and C–C′, translating between sections along the western Jishi Shan back thrust (Figures 4 and 6). We also include an additional 15 km of undeformed cross-sectional length on each end of the composite regional cross section (total of 30 km) when calculating average regional shortening %. This addition reflects the average spacing of major structures (~40 km) and is included to accurately portray the average regional shortening. This approach indicates 11% (19 km) shortening with our composite, deformed state cross section measuring 145 km long and our "undeformed" or restored cross section measuring 164 km long. We calculate shortening uncertainties across our composite east-west cross section by (1) taking into account the maximum and minimum allowed throw across faults (described in section 4.3) and (2) allowing near-surface fault dips to vary by ±5°. This combination gives maximum and minimum shortening of 22 km (13%) and 16 km (10%).

5. Results for NNE-SSW Cross Sections

[28] The structural geology along a NNE-SSW transect across our study area is dominated by the West Qinling and

Laji Shan reverse faults, which are separated by ~60 km across strike and bracket our east-west sections. We constructed short cross sections across these ranges where detailed hanging wall thermochronology and footwall magnetostratigraphy constrain the magnitude of fault offset.

5.1. West Qinling Reverse Fault

[29] We estimate West Qinling fault offset and shortening by restoring a surface identified on both the hanging wall and footwall that is of common age and character (Figure 9). *Clark et al.* [2010] report 14 AHe ages collected at different depths below a low-relief, exhumed unconformity surface on the West Qinling hanging wall that, together, compromise a 2600 m thick AHe age-depth profile below this surface. *Clark et al.* [2010] projected these ages—collected at distances of 3.5 to 17 km away from the surface trace of the West Qinling fault and over a 50 km distance along strike—onto a common cross section to define AHe isochrons. The top of the hanging wall unconformity surface has a cooling age of ~110 Ma, and a downward transition to more closely spaced isochrons starting at ~45 Ma is interpreted to signal the onset of rapid cooling due to thrust-induced rock uplift and erosion of the hanging wall. On the West Qinling footwall, the basement-cover unconformity also has an AHe cooling age of ~110 Ma where it is exposed 33 km to the north of the fault. These correlative ~110 Ma ages suggest that the hanging wall and footwall unconformity surfaces were once continuous and thereby provide an offset marker across the fault.

[30] Whereas the unconformity surface is clearly exposed on the West Qinling hanging wall and can reliably be projected to the location of the fault plane, the position of the equivalent basement-cover unconformity on the footwall is inferred from magnetostratigraphy (Figure 9). Oligocene-Pleistocene sedimentary successions deposited on the footwall of the West Qinling fault have thicknesses of ~3000 m and ~1200 m in the Xunhua and Linxia basins, respectively [*Fang et al.*, 2003; *Hough et al.*, 2011; *Lease et al.*, 2012]. Adjacent to the West Qinling range front, where flexural subsidence is predicted to be greatest, stratigraphic thicknesses may be even larger [*Fang et al.*, 2003]. Within this 1200–3000 m range of thickness estimates and taking into account different stratigraphic positions exposed on the footwall along the 50 km length of the fault examined by thermochronology, we use a stratigraphic thickness of ~1800 m on the footwall in our cross section construction. Our cross section follows the profile of *Clark et al.* [2010], but is generalizable to areas west along strike of the West Qinling fault bordering Xunhua basin (Figure 2).

[31] The once-continuous basement-cover unconformity is now vertically offset across the West Qinling fault by 4.3 km (Figure 9). At the surface, exposures of the fault plane at several locations reveals dips of 45–50° [*Duvall et al.*, 2011; *GBGMR*, 1991; *QBGMR*, 1991] and suggest that shortening is commensurate with fault throw, such that shortening totals ~4.3 km. Minor back-tilting of inferred AHe isochrons by ~4° (Figure 9) [*Clark et al.*, 2010] suggests a small magnitude of fault concavity at depth, though this geometry does not alter our estimate of shortening. Taking into account uncertainties associated with the 45–50° range of fault dips and the 1200–3000 m range of footwall stratigraphic thicknesses, the West Qinling data are compatible with a 3.1–5.5 km range of shortening.

5.2. Laji Shan Reverse Fault

[32] We estimate offset and shortening across the eastern Laji Shan fault by restoring the basement-cover unconformity across the fault (Figure 10). The position of this now eroded surface on the hanging wall is constrained by low-temperature thermochronology from a 900 m relief transect that characterizes the exhumation history of the hanging wall [*Lease et al.*, 2011]. *Lease et al.* [2011] report six thermochronology samples that were collected from the hanging wall within 1–3 km of the surface trace of the Laji Shan fault. These samples span only 2 km along fault strike such that they are naturally aligned along a common cross section and need not be projected over large distances. A narrow, 23–18 Ma range of AHe ages from the hanging wall block defines an early Miocene interval of rapid cooling, whereas a much wider, 71–37 Ma range of apatite fission track (AFT) ages from the same samples defines an early Cenozoic period of slower cooling. The combined AHe and AFT age-elevation data suggest 60° of rapid cooling since ~22 Ma and, hence, removal of ~3 km of rock in Neogene time [*Lease et al.*, 2011]. This erosion reflects both unroofing of a low-geothermal gradient Mesozoic and Cenozoic sedimentary cover from the range, as well as erosion of higher-geothermal gradient basement rock (Figure 10). Nearby magnetostratigraphy and biostratigraphy indicate ~1000 m of Mesozoic strata [*Horton et al.*, 2004] and ~800 m of Paleogene strata [*Dai et al.*, 2006; *Lease et al.*, 2012] in this area.

[33] The footwall of the Laji Shan fault in the Xining-Linxia basin contains the same ~1800 m thickness of Mesozoic plus Paleogene strata identified on the hanging wall, as well as an additional ~1000 m of Neogene strata (Figure 10) [*Fang et al.*, 2003]. The Laji Shan fault is poorly exposed and its dip is only weakly constrained, with one 30° measurement located 27 km along strike of the fault to the west of our cross section [*QBGMR*, 1991]. Given the style of faulting in this area, however, we interpret that slip on a steeper fault, dipping ~45°, is more likely responsible for exhumation of the hanging wall rocks along our structural and thermochronological transect (Figure 10). The throw of the basement-cover unconformity across the Laji Shan fault is ~5.1 km, which equates to an equivalent amount of shortening for a 45° dipping fault. Acknowledging uncertainty associated with the orientation of the fault plane, a 35–55° range of dips equates with a 3.6–7.3 km range of shortening. Uncertainties in stratigraphic thicknesses along the Laji Shan fault, on the other hand, have a less than 10% effect on the shortening estimate because similar strata are found on both the hanging wall and footwall.

5.3. NNE-SSW Restoration

[34] We link our cross sections across the two principal NNE vergent structures in this area, the West Qinling and Laji Shan faults (Figures 9 and 10), into a longer regional section to provide a minimum estimate of NNE-SSW shortening. This approach does not take into account additional shortening across subsidiary NNE vergent or SSW vergent structures in the intervening 60 km between the two ranges, but our observations and previous mapping [*GBGMR*, 1991; *QBGMR*, 1991] suggest only minor NNE vergent or SSW

vergent folding in this zone. This approach also avoids structural complications created by later middle Miocene to Recent east-west shortening, e.g., Figures 4–6. We calculate NNE-SSW shortening across a 100 km long section that encompasses our entire D–D′ and E–E′ cross sections and extends an additional 20 km into the Xining basin north of E′. This addition is included to accurately portray average regional shortening %. We conservatively estimate 9.4 km of shortening along this section, which equates to 9% shortening. The uncertainties concerning fault dips and stratigraphic thicknesses conspire to give minimum and maximum shortening estimates of 6.7 km (6%) and 12.8 km (11%). Additional shortening across other structures in the region between the West Qinling and Laji Shan faults would increase these estimates of shortening.

6. Discussion

6.1. Timing of Shortening

[35] Several lines of evidence from the east vergent Jishi Shan and adjacent basins (Figure 2) suggest that east-west shortening in our study area did not commence until middle Miocene time: (1) low-temperature thermochronological age-elevation data from the Jishi Shan hanging wall show the onset of rapid cooling due to thrust-induced rock uplift and erosion at ∼13 Ma [*Lease et al.*, 2011]; (2) Local paleoclimate records from the $\delta^{18}O$ of calcareous basin fill suggest topographic isolation of the Xunhua and Linxia basins by surface uplift of the intervening Jishi Shan by ∼11 Ma, but not before ∼16 Ma [*Dettman et al.*, 2003; *Fan et al.*, 2007; *Hough et al.*, 2011]; (3) sedimentary rocks in Linxia basin show a doubling of Jishi Shan-derived zircons by 11.5 Ma that indicates enhanced erosion of Jishi Shan basement rock by this time [*Lease et al.*, 2012]; and (4) magnetostratigraphic records from northern Xunhua basin show a 50% acceleration in sediment accumulation rates starting at ∼12 Ma, presumably due to enhanced erosion of the growing Jishi Shan [*Lease et al.*, 2012].

[36] To the west of the Jishi Shan, precise constraints on the timing of fault movement for the north trending Gongbo Shan and Zamazari Shan faults have yet to be established (Figures 2, 4, and 5). Disruption of the E3 unit across our cross sections indicates that east-west shortening must postdate the Oligocene deposition of this unit. Mesozoic AHe ages from the hanging walls of the Gongbo Shan and Zamazari Shan faults indicate that burial reheating of the basement by Cenozoic deposition and later unroofing of the hanging wall was insufficient in magnitude to expose reset Cenozoic AHe ages at the surface today. Thermochronologic systems with even lower effective closure temperatures like $^{4}He/^{3}He$ [*Shuster and Farley*, 2005] are better suited to capture the onset of faults like the Gongbo Shan and Zamazari Shan where hanging wall erosion is <2–3 km. Given that the structural positions of the Gongbo Shan and Zamazari Shan are similar to that of the Jishi Shan (Figure 2), where movement is documented to accelerate after ∼13 Ma, we infer that all three ranges became active either during or after middle Miocene time.

[37] In addition to 11% east-west shortening in middle Miocene to Recent time, our study area in northeastern Tibet was also subject to 9% NNE-SSW shortening. The onset of movement on structures accommodating NNE-SSW shortening is well constrained along the two principal NNE vergent structures in this area: the West Qinling and eastern Laji Shan reverse faults (Figures 9 and 10). Thermochronologic age-elevation data from the hanging walls of each structure show a transition to rapid cooling due to thrust-induced rock uplift and erosion at ∼45–50 for the West Qinling [*Clark et al.*, 2010] and at ∼22 Ma for the Laji Shan [*Lease et al.*, 2011]. In addition, dating of West Qinling fault gouge suggests an onset of faulting at 50 ± 8 Ma [*Duvall et al.*, 2011]. Finally, nearby sedimentary basins corroborate accelerated erosion at and after these times.

[38] Magnetostratigraphic records from northern Xunhua basin concur with early Miocene intensification of Laji Shan faulting: they display a more than twofold acceleration in sediment accumulation and basin subsidence during 24–21 Ma, as well as a transition to alluvial facies at 20 Ma that is nearly coincident with intensified erosion of basement rock in the Laji Shan by 19 Ma [*Lease et al.*, 2012]. The onset of deposition in Xining basin at ∼52 Ma [*Dai et al.*, 2006] and a ∼25° clockwise rotation in the basin by ∼41 Ma [*Dupont-Nivet et al.*, 2008] corroborate early Cenozoic deformation in northeastern Tibet at this time.

[39] We interpret NNE-SSW shortening, active in this region since at least ∼45 Ma [*Clark et al.*, 2010; *Duvall et al.*, 2011], to diminish significantly in magnitude after middle Miocene time when east-west shortening initiated. Thermochronology from the NNE vergent eastern Laji Shan indicates that rapid cooling of the range due to accelerated reverse faulting was largely over by middle Miocene time [*Lease et al.*, 2011]. Thermal modeling of apatite fission track and apatite (U-Th)/He age-elevation data suggest 60°C of rapid cooling of the Laji Shan hanging wall from 23 to 21 Ma until 18–15 Ma, but only minimal exhumation (10°C of cooling) from 15 Ma until the present day [*Lease et al.*, 2011]. In addition, foreland basin subsidence provides a useful record of fault activity because rock uplift is observed to outpace erosion everywhere in this arid study area. Subsidence rates in northern Xunhua basin adjacent to the eastern Laji Shan decrease fourfold by middle Miocene time and suggest diminished flexural loading of the basin and, hence, diminished Laji Shan reverse faulting by this time [*Lease et al.*, 2012]. Slip on the West Qinling fault continued after middle Miocene time, but likely incorporated significant left-lateral strike-slip motion [*Wang et al.*, 2012]. In our subsequent calculations of shortening rates and crustal thickening magnitudes, we approximate NNE-SSW shortening to be restricted to the middle Eocene to middle Miocene period, after which time east-west shortening initiated and was dominant. The modern GPS velocity field in this area is east directed (relative to stable Eurasia), whereas the modeled strain rate field has an ENE-WSW contractional direction (Figure 11) [*Gan et al.*, 2007].

6.2. Accelerated Shortening Since Middle Miocene Time

[40] Our cross-section reconstructions suggest that although reverse faulting commenced on the northeastern margin of Tibet shortly after India-Asia collision at ∼50 Ma, more than half of the net Cenozoic crustal shortening and thickening of this area has occurred since only ∼13 Ma (Figure 12). At ∼13 Ma, shortening rates accelerate fivefold: an average middle Miocene to Recent east-west shortening

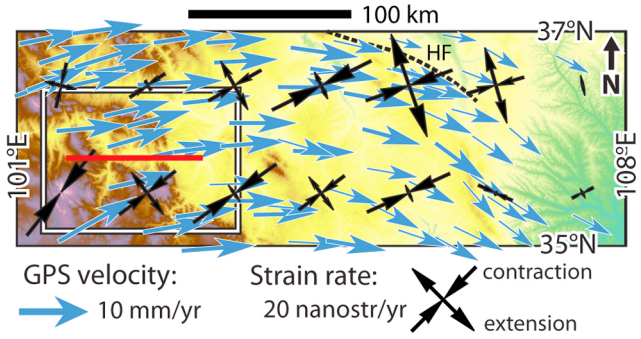

Figure 11. Modern strain rate field for the northeastern Tibetan Plateau derived from Global Positioning System (GPS) velocities [*Gan et al.*, 2007]. GPS velocities displayed relative to stable Eurasia. Note the east directed GPS velocity field and ENE-WSW contractional field in our study area, which supports our interpretation of east-west shortening in middle Miocene to Recent time. Red line denotes our composite east-west cross section (Figures 4 and 6), whereas the white box denotes the location of Figure 2. HF, Haiyuan strike-slip fault, denoted by dotted line.

rate of 1.5 ± 0.2 mm/yr can be contrasted with a middle Eocene to middle Miocene NNE-SSW shortening rate of 0.3 ± 0.1 mm/yr (Table 2). For comparison, the modern geodetic shortening rates measured along ~300 km long, generally E-W profiles across the northeastern plateau margin are 3.6–5.6 ± 2 mm/yr [*Zheng et al.*, 2012; *Zhang et al.*, 2004]. Over ~150 km long profiles equivalent to our middle Miocene to Recent shortening profile in distance but 15° different in orientation, the geodetic shortening rates of ~1.8–2.8 mm/yr (Table 2) are in approximate agreement to or slightly greater than our estimated shortening rate of 1.5 mm/yr over the last 13 Myr. The generally east directed GPS velocity field and ENE-WNW contractional strain field in our study area (Figure 11) [*Gan et al.*, 2007] suggest that north striking faults, such as the Jishi Shan reverse fault (Figure 2), are oriented approximately orthogonal to modern convergence.

6.3. Crustal Thickening

[41] We utilize our determinations of percent shortening along our east-west and NNE-SSW structural transects that overlap in areal extent to place some bounds on the crustal thickening history along the northeastern margin of the Tibetan Plateau near 36°N 102.5°E (Figure 12 and Table 2). To evaluate the contribution of horizontal crustal shortening to vertical thickening of the crustal column, we make the following simplifying assumptions: (1) the volume of crust behaved as a closed system with no material gained from or lost to adjacent regions of the plateau, (2) the principal shortening strain was oriented parallel to the line of the cross sections (e.g., plane strain), and (3) crustal thickening was vertically uniform (e.g., pure shear) such that the shortening

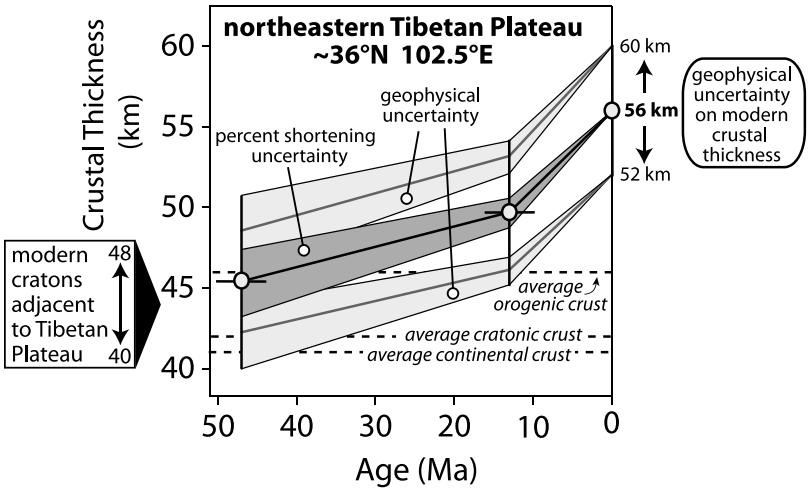

Figure 12. Plot of estimated crustal thickness versus age for the northeastern Tibetan Plateau based on restoration of the modern crustal thickness (56 ± 4 km) [*Pan and Niu*, 2011] that accounts for 11 $^{+2}/_{-1}$% east-west shortening in middle Miocene to Recent time and 9 $^{+2}/_{-3}$% NNE-SSW shortening in middle Eocene–middle Miocene time. Volumetric calculations made on a 145 km × 100 km modern crustal area and 56 km thickness. Percent shortening uncertainties reflect (1) the maximum and minimum vertical offsets across faults that are permissible based on magnetostratigraphic, thermochronological, and other constraints; and (2) the ± 5–10° range of near-surface fault dips—see sections 4 and 5 for details. The geophysical uncertainty on modern crustal thickness reflects both the resolution of individual receiver function analyses and the range of modern crustal thickness estimates from different stations in this area [*Pan and Niu*, 2011] (Figure 2). Our estimate of crustal thickness before India-Asia collision, 45 ± 5 km, is similar to the 44 ± 4 km modern crustal thickness of stable cratonic regions adjacent to the Tibetan Plateau in the Tarim, Ordos, and Sichuan basins (see section 6.3 for details and references), as well as the average thicknesses of weighted global continental crust (41 ± 6 km), cratonic crust (42 ± 6 km), and orogenic crust (46 ± 10 km) [*Christensen and Mooney*, 1995]. We interpret this equivalence to obviate lower crustal flow as a necessary Cenozoic thickening agent for the northeastern Tibetan Plateau.

Table 2. Cross Section Restoration Results

Interval	Shortening Direction	Shortening (%)	Shortening Rate (mm/yr)	Crustal Thickness (km)	Thickness Change (km)
Modern (geodetic)	ESE-WSW	-	1.8 ± 1[a]	56 ± 4[c]	-
	ENE-WNW	-	2.8 ± 1[b]		
Middle Miocene–Recent	East-West	11 (10–13)	1.5 ± 0.2	50 ± 4	6
Middle Eocene–Middle Miocene	NNE-SSW	9 (6–11)	0.3 ± 0.1	45 ± 5	5

[a][*Zheng et al.*, 2012].
[b][*Zhang et al.*, 2004].
[c][*Pan and Niu*, 2011].

of the uppermost crust that we have measured at the surface defines the amount of shortening at all depths in the crust. Additional crustal thickening accomplished by potential flow of lower crustal material that is decoupled from upper crustal shortening (Poiseuille-type flow, after *Bird* [1991] and *Clark and Royden* [2000]) would augment our crustal thickening estimates.

[42] One source of uncertainty in our analysis of Cenozoic crustal thickening is our assumption of east-west plane strain during middle Miocene to Recent shortening, and NNE-SSW plane strain during middle Eocene–middle Miocene shortening. In support of assumed east-west plane strain, the modern east directed GPS velocity field and ENE-WSW contractional strain rate field in our study area (Figure 11) are consistent with east-west shortening in middle Miocene to Recent time. Furthermore, shortening structures with significant growth during middle Miocene to Recent time trend north, and we have no evidence for significant oblique slip on these structures. Slight deviation in the strikes of some Cenozoic beds from the north or south direction (Figure 3) may reflect differential shortening, plunging folds, or minor oblique slip. Assumed Eocene NNE-SSW plane strain is harder to evaluate given its later disruption by the more recent east-west shortening strain. Our assumption of NNE-SSW shortening is supported by the generally WNW trend of structures that were active in middle Eocene–middle Miocene time, as well as by the cessation of NNE vergent reverse faulting documented for some of these structures in early Miocene time [*Lease et al.*, 2011]. Based on this reasoning, we argue that our assumptions of plane strain do not introduce significant uncertainty. Finally, we note that even if our estimated shortening strain is oblique to some axis of greater shortening, then this scenario would argue that our estimated shortening is a minimum. A greater shortening strain of a slightly different orientation than that which we assume would argue for an even thinner initial crust, and hence more crustal thickening could be attributed to shortening in the absence of lower crustal flow.

[43] We calculate what the crustal thickness of northeastern Tibet would be once Cenozoic crustal shortening is restored (Figure 12), using the modern 56 ± 4 km crustal thickness of our study area in northeastern Tibet (Figure 2) [*Liu et al.*, 2006; *Pan and Niu*, 2011] and the modern areal extent of the study area (145 km × 100 km) as starting points. These volumetric calculations suggest that prior to east-west shortening in middle Miocene to Recent time, the crust in our study area of northeastern Tibet was 50 ± 4 km thick or about 6 km (~11%) thinner than at present (Figure 12 and Table 2). Simple Airy isostatic calculations for a crustal thickness change of 6 km predict that the elevation in this area was ~0.8–1.1 km lower in middle Miocene time compared to today, using a range of crustal (2700–2800 kg/m^3) and mantle (3200–3300 kg/m^3) densities. The modest paleoelevation change that Airy isostasy predicts, unfortunately, falls within the uncertainties of all Tibetan paleoaltimetric studies [e.g., *Garzione et al.*, 2000; *Molnar et al.*, 2010, and references therein; *Rowley et al.*, 2001]. Miocene-Recent changes in the paleoevalation of northeastern Tibet, therefore, may not be detectable using standard, isotope-based techniques. Our estimate of the crustal thickness in this area before the onset of India-Asia collision at ~50 Ma, on the other hand, is 45 ± 5 km (Figure 12 and Table 2). This precollision estimate takes the middle Miocene crustal thickness estimate and restores the 9% NNE-SSW shortening that occurred in middle Eocene to middle Miocene time. Airy isostasy predicts a middle Eocene elevation ~1.4–2 km lower than today.

[44] Evaluating the role of lower crustal flow as a Cenozoic crustal thickening agent in northeastern Tibet depends critically on the true thickness of northeastern Tibetan crust prior to the middle Eocene onset of shortening. Unfortunately, the pre-Eocene thickness of northeastern Tibetan crust is not independently constrained. Upper Jurassic through upper Cretaceous deposits in northeastern Tibet are all terrestrial in character [*Horton et al.*, 2004; *Ritts and Biffi*, 2001] and suggest that the crust must have been at the very least 32–35 km thick at this time to have been above sea level. Furthermore, the suturing of various terranes onto the Sino-Korean craton in Paleozoic and Mesozoic time likely thickened the crust in northeastern Tibet before Cenozoic time, especially in our study area astride the south Qilian suture zone. In addition, up to 60% Cretaceous shortening in southern and central Tibet [*Kapp et al.*, 2005, 2007; *Murphy et al.*, 1997] suggest significant crustal thickening in parts of the Tibetan Plateau in a retroarc setting immediately preceding India-Asia continental collision. Debate continues, however, whether Cretaceous basins in and near our study area in northeastern Tibet are contractional [*Craddock et al.*, 2012] or transtensional [*Horton et al.*, 2004; *Vincent and Allen*, 1999] in origin, or whether they transition from the former mode to the latter toward the north.

[45] Our reconstructed Eocene crustal thickness for the northeastern Tibetan Plateau, on the other hand, is comparable to modern crustal thicknesses both globally and adjacent to the plateau. Our reconstructed Eocene thickness (45 ± 5 km) matches, within uncertainty, the average thicknesses of weighted global continental crust (41 ± 6 km), cratonic crust (42 ± 6 km), and orogenic crust (46 ± 10 km) [*Christensen and Mooney*, 1995]. Furthermore, our estimate of the middle Eocene crustal thickness for

northeastern Tibet (45 ± 5 km) matches modern crustal thicknesses determined via receiver functions and seismic refraction for stable, cratonal regions adjacent to the Tibetan Plateau (44 ± 4 km; Figure 1), such as in the Tarim (42, 43, 48 km, from, respectively, *Kao et al.* [2001], *Qiusheng et al.* [2002], and *Zhao et al.* [2006]), Ordos (40, 42, 43 km, from, respectively, *Chen et al.* [2005], *Liu et al.* [2006], and *Pan and Niu* [2011]), and Sichuan basins (43, 43, 44, 44–48, 48 km, from, respectively, *Robert et al.* [2010], *Wang et al.* [2007, 2010a, 2010b], and *Xu et al.* [2007]). Although the crust of these regions is much older and stronger than Tibetan crust [*Molnar and Tapponnier*, 1981], the immunity of these cratons to Mesozoic and Cenozoic orogeny suggests that the modern thickness of stable, undeformed regions surrounding the plateau provides one estimate of the thickness of northeastern Tibet prior to India-Asia collision.

[46] The equivalence of the reconstructed Eocene crustal thickness in our study area with modern crustal thicknesses both globally and adjacent to the Tibetan Plateau suggests that Cenozoic crustal shortening in northeastern Tibet can account for the modern, moderately thickened crust without resorting either to lower crustal flow or to a previously thickened crust before Cenozoic deformation began. Hence, Poiseuille flow of lower crustal material is apparently unnecessary to account for crustal thickening in this sector of northeastern Tibet.

[47] Our finding obviating lower crustal flow agrees with both geophysical studies of northeastern Tibet as well as structural studies of adjacent sectors of the plateau. Locally, our result concurs with a recent receiver function study that interprets the low Poisson's ratio (0.240) beneath the northeastern Tibetan Plateau to indicate a dominantly felsic crustal column without flow and addition of mafic lower crust [*Pan and Niu*, 2011]. Furthermore, using geodetic and geologic data collected near the Kunlun Fault, *Hilley et al.* [2005] estimate the viscosity of the middle to lower crust beneath northern Tibet to be orders of magnitude larger (10^{19}–10^{21} Pa s) than that required for channel flow (10^{16}–10^{18} Pa s). Finally, a growing number of balanced cross sections across the margins of the Tibetan Plateau document Cenozoic shortening sufficient to generate modern crustal thicknesses: in northern Tibet [*Yin et al.*, 2007, 2008a, 2008b], eastern Tibet [*Hubbard and Shaw*, 2009], and northeastern Tibet (this paper). Collectively, these similar findings suggest that lower crustal flow is either unnecessary to account for Cenozoic crustal thickening beneath the outer margins of the Tibetan Plateau or, alternatively, has a much more restricted role than originally proposed (Figure 1) [*Clark and Royden*, 2000].

7. Conclusion

[48] Balanced reconstructions of Cenozoic crustal shortening along 100 to 145 km long cross sections across the northeastern margin of the Tibetan Plateau near 36°N 102.5°E indicate 11 $^{+2}/_{-1}$% east-west shortening and 9 $^{+2}/_{-3}$% NNE-SSW shortening. The onset of accelerated cooling on the hanging walls of major reverse faults indicates that NNE-SSW shortening began in middle Eocene time shortly after initial India-Asia collision. East-west shortening, however, did not commence until ~35 Myr later. Furthermore, magnetostratigraphic records of basin filling and provenance corroborate long-standing NNE-SSW contraction that is followed by a kinematic shift in middle Miocene time. We detect a fivefold acceleration in crustal shortening rates in middle Miocene to Recent time that accounts for more than half of the total Cenozoic crustal shortening and thickening in this region. Collectively, these observations suggest that the mean elevation in this region was ~1 km lower before middle Miocene time.

[49] Assuming shortening measured at the surface defines shortening at all depths in the crust, we reconstruct the modern 56 ± 4 km crustal thickness of this region to have had a middle Miocene thickness of 50 ± 4 km and a middle Eocene thickness of 45 ± 5 km. Although independent estimates of the middle Eocene thickness are lacking, the similarity of our estimated thickness with modern continental crustal thicknesses both globally and adjacent to the Tibetan Plateau suggests that Cenozoic thickening of this region was accomplished primarily by crustal shortening.

[50] **Acknowledgments.** We thank Ken Farley and Lindsey Hedges for apatite (U-Th)/He analyses, Peizhen Zhang for facilitating fieldwork, Laura Smith and Cecile Bonnet-Matzinger for field assistance, Michael Oskin for his review, and Peter Molnar for comments on an earlier version of this paper. This work was funded jointly by the U.S. National Science Foundation Continental Dynamics program (grant EAR-0507431), a U.S. National Science Foundation Graduate Research Fellowship to R.O. Lease, the National Science Foundation of China (grant 41030317), and the China State Key Laboratory of Earthquake Dynamics (grant LED2009A06). We acknowledge Midland Valley Exploration for providing 2-D Move software through their Academic Software Initiative.

References

Amos, C. B., D. W. Burbank, D. C. Nobes, and S. A. L. Read (2007), Geomorphic constraints on listric thrust faulting: Implications for active deformation in the Mackenzie Basin, South Island, New Zealand, *J. Geophys. Res.*, *112*, B03S11, doi:10.1029/2006JB004291.

Beck, R. A., et al. (1995), Stratigraphic evidence for an early collision between northwest India and Asia, *Nature*, *373*(6509), 55–58, doi:10.1038/373055a0.

Bird, P. (1991), Lateral extrusion of lower crust from under high topography, in the isostatic limit, *J. Geophys. Res.*, *96*(B6), 10,275–10,286.

Bovet, P. M., B. D. Ritts, G. Gehrels, A. O. Abbink, B. Darby, and J. Hourigan (2009), Evidence of Miocene crustal shortening in the north Qilian Shan from Cenozoic stratigraphy of the western Hexi corridor, Gansu Province, China, *Am. J. Sci.*, *309*(4), 290–329, doi:10.2475/00.4009.02.

Braitenberg, C., M. Zadro, J. Fang, Y. Wang, and H. T. Hsu (2000), The gravity and isostatic Moho undulations in Qinghai-Tibet Plateau, *J. Geodyn.*, *30*(5), 489–505, doi:10.1016/S0264-3707(00)00004-1.

Burbank, D. W., J. K. McLean, M. Bullen, K. Y. Abdrakhmatov, and M. M. Miller (1999), Partitioning of intermontane basins by thrust-related folding, Tien Shan, Kyrgyzstan, *Basin Res.*, *11*(1), 75–92, doi:10.1046/j.1365-2117.1999.00086.x.

Burchfiel, B. C., C. Zhiliang, L. Yupinc, and L. H. Royden (1995), Tectonics of the Longmen Shan and adjacent regions, central China, *Int. Geol. Rev.*, *37*(8), 661–735, doi:10.1080/00206819509465424.

Chen, J. H., Q. Y. Liu, S. C. Li, B. Guo, and Y. G. Lai (2005), Crust and upper mantle *S*-wave velocity structure across northeastern Tibetan Plateau and Ordos block, *Chin. J. Geophys.*, *48*(2), 369–379.

Chen, Y. T., L. S. Xu, X. Li, and M. Zhao (1996), Source process of the 1990 Gonghe, China, earthquake and tectonic stress field in the northeastern Qinghai-Xizang (Tibetan) Plateau, *Pure Appl. Geophys.*, *146*(3–4), 697–715, doi:10.1007/BF00874741.

Christensen, N. I., and W. D. Mooney (1995), Seismic velocity structure and composition of the continental crust—A global view, *J. Geophys. Res.*, *100*(B6), 9761–9788.

Clark, M. K., and L. H. Royden (2000), Topographic ooze: Building the eastern margin of Tibet by lower crustal flow, *Geology*, *28*(8), 703–706.

Clark, M. K., J. W. M. Bush, and L. H. Royden (2005), Dynamic topography produced by lower crustal flow against rheological strength heterogeneities bordering the Tibetan Plateau, *Geophys. J. Int.*, *162*(2), 575–590, doi:10.1111/j.1365-246X.2005.02580.x.

Clark, M. K., K. A. Farley, D. Zheng, Z. C. Wang, and A. Duvall (2010), Early Cenozoic faulting on the northern Tibetan Plateau margin from

apatite (U-Th)/He ages, *Earth Planet. Sci. Lett.*, *296*, 78–88, doi:10.1016/j.epsl.2010.04.051.

Craddock, W. H., E. Kirby, N. W. Harkins, H. P. Zhang, X. H. Shi, and J. H. Liu (2010), Rapid fluvial incision along the Yellow River during headward basin integration, *Nat. Geosci.*, *3*(3), 209–213, doi:10.1038/ngeo777.

Craddock, W. H., E. Kirby, D. Zheng, and J. Liu (2012), Tectonic setting of Cretaceous basins on the NE Tibetan Plateau: Insights from the Jungong basin, *Basin Res.*, *24*(1), 51–69, doi:10.1111/j.1365-2117.2011.00515.x.

Dahlstrom, C. D. A. (1969), Balanced cross-sections, *Can. J. Earth Sci.*, *6*, 743–757, doi:10.1139/e69-069.

Dai, S., X. M. Fang, G. Dupont-Nivet, C. H. Song, J. P. Gao, W. Krijgsman, C. Langereis, and W. L. Zhang (2006), Magnetostratigraphy of Cenozoic sediments from the Xining Basin: Tectonic implications for the northeastern Tibetan Plateau, *J. Geophys. Res.*, *111*, B11102, doi:10.1029/2005JB004187.

Dettman, D. L., X. M. Fang, C. N. Garzione, and J. J. Li (2003), Uplift-driven climate change at 12 Ma: A long δO^{18} record from the NE margin of the Tibetan Plateau, *Earth Planet. Sci. Lett.*, *214*(1–2), 267–277, doi:10.1016/S0012-821X(03)00383-2.

Dupont-Nivet, G., P. Andriessen, J. Juez-Larre, J. Foeken, and X. Jiang (2007), Middle Miocene exhumation of the Laji Shan, northeastern Tibetan Plateau, *Eos Trans. AGU*, *88*(52), Fall Meet. Suppl., Abstract T12D05.

Dupont-Nivet, G., S. Dai, X. Fang, W. Krijgsman, V. Erens, M. Reitsma, and C. Langereis (2008), Timing and distribution of tectonic rotations in the northeastern Tibetan Plateau, *Geol. Soc. Am. Spec. Pap.*, *444*, 73–87.

Duvall, A. R., and M. K. Clark (2010), Dissipation of fast strike-slip faulting within and beyond northeastern Tibet, *Geology*, *38*(3), 223–226, doi:10.1130/G30711.1.

Duvall, A. R., M. K. Clark, B. van der Pluijm, and C. Y. Li (2011), Direct dating of Eocene reverse faulting in northeastern Tibet using Ar-dating of fault clays and low-temperature thermochronometry, *Earth Planet. Sci. Lett.*, *304*(3–4), 520–526, doi:10.1016/j.epsl.2011.02.028.

Ehlers, T. A. (2005), Crustal thermal processes and the interpretation of thermochronometer data, *Rev. Mineral. Geochem.*, *58*(1), 315–350, doi:10.2138/rmg.2005.58.12.

Erslev, E. A. (1986), Basement balancing of Rocky Mountain foreland uplifts, *Geology*, *14*(3), 259–262, doi:10.1130/0091-7613(1986)14<259:BBORMF>2.0.CO;2.

Erslev, E. A. (1991), Trishear fault-propagation folding, *Geology*, *19*(6), 617–620, doi:10.1130/0091-7613(1991)019<0617:TFPF>2.3.CO;2.

Fan, M. J., D. L. Dettman, C. H. Song, X. M. Fang, and C. N. Garzione (2007), Climatic variation in the Linxia basin, NE Tibetan Plateau, from 13.1 to 4.3 Ma: The stable isotope record, *Palaeogeogr. Palaeoclimatol. Palaeoecol.*, *247*(3–4), 313–328, doi:10.1016/j.palaeo.2006.11.001.

Fang, X. M., C. Garzione, R. Van der Voo, J. J. Li, and M. J. Fan (2003), Flexural subsidence by 29 Ma on the NE edge of Tibet from the magnetostratigraphy of Linxia Basin, China, *Earth Planet. Sci. Lett.*, *210*(3–4), 545–560, doi:10.1016/S0012-821X(03)00142-0.

Fang, X. M., M. D. Yan, R. Van der Voo, D. K. Rea, C. H. Song, J. M. Pares, J. P. Gao, J. S. Nie, and S. Dai (2005), Late Cenozoic deformation and uplift of the NE Tibetan Plateau: Evidence from high-resolution magneto stratigraphy of the Guide basin, Qinghai Province, China, *Geol. Soc. Am. Bull.*, *117*(9–10), 1208–1225, doi:10.1130/B25727.1.

Farley, K. A., R. A. Wolf, and L. T. Silver (1996), The effects of long alpha-stopping distances on (U-Th)/He ages, *Geochim. Cosmochim. Acta*, *60*(21), 4223–4229, doi:10.1016/S0016-7037(96)00193-7.

Flowers, R. M., R. A. Ketcham, D. L. Shuster, and K. A. Farley (2009), Apatite (U-Th)/He thermochronometry using a radiation damage accumulation and annealing model, *Geochim. Cosmochim. Acta*, *73*(8), 2347–2365, doi:10.1016/j.gca.2009.01.015.

Galvé, A., A. Hirn, J. A. Mei, J. Gallart, B. de Voogd, J. C. Lepine, J. Diaz, Y. X. Wang, and Q. A. Hui (2002), Modes of raising northeastern Tibet probed by explosion seismology, *Earth Planet. Sci. Lett.*, *203*(1), 35–43, doi:10.1016/S0012-821X(02)00863-4.

Gan, W. J., P. Z. Zhang, Z. K. Shen, Z. J. Niu, M. Wang, Y. G. Wan, D. M. Zhou, and J. Cheng (2007), Present-day crustal motion within the Tibetan Plateau inferred from GPS measurements, *J. Geophys. Res.*, *112*, B08416, doi:10.1029/2005JB004120.

Garzanti, E., and T. Van Haver (1988), The Indus clastics: Fore-arc basin sedimentation in the Ladakh Himalaya (India), *Sediment. Geol.*, *59*(3–4), 237–249, doi:10.1016/0037-0738(88)90078-4.

Garzione, C. N., J. Quade, P. G. DeCelles, and N. B. English (2000), Predicting paleoelevation of Tibet and the Himalaya from δO^{18} vs. altitude gradients in meteoric water across the Nepal Himalaya, *Earth Planet. Sci. Lett.*, *183*(1–2), 215–229, doi:10.1016/S0012-821X(00)00252-1.

Gansu Provincial Bureau of Geology and Mineral Resources (1991), *Regional Geology of the Gansu Province*, Geol. Publ., Beijing.

Harkins, N., E. Kirby, A. Heimsath, R. Robinson, and U. Reiser (2007), Transient fluvial incision in the headwaters of the Yellow River, northeastern Tibet, China, *J. Geophys. Res.*, *112*, F03S04, doi:10.1029/2006JF000570.

Hilley, G. E., R. Burgmann, P. Z. Zhang, and P. Molnar (2005), Bayesian inference of plastosphere viscosities near the Kunlun fault, northern Tibet, *Geophys. Res. Lett.*, *32*, L01302, doi:10.1029/2004GL021658.

Horton, B. K., G. Dupont-Nivet, J. Zhou, G. L. Waanders, R. F. Butler, and J. Wang (2004), Mesozoic-Cenozoic evolution of the Xining-Minhe and Dangchang basins, northeastern Tibetan Plateau: Magnetostratigraphic and biostratigraphic results, *J. Geophys. Res.*, *109*, B04402, doi:10.1029/2003JB002913.

Hough, B. G., C. N. Garzione, Z. C. Wang, R. O. Lease, D. W. Burbank, and D. Y. Yuan (2011), Stable isotope evidence for topographic growth and basin segmentation: Implications for the evolution of the NE Tibetan Plateau, *Geol. Soc. Am. Bull.*, *123*(1–2), 168–185, doi:10.1130/B30090.1.

Hu, S. B., L. J. He, and J. Y. Wang (2000), Heat flow in the continental area of China: A new data set, *Earth Planet. Sci. Lett.*, *179*(2), 407–419, doi:10.1016/S0012-821X(00)00126-6.

Hubbard, J., and J. H. Shaw (2009), Uplift of the Longmen Shan and Tibetan Plateau, and the 2008 Wenchuan (M = 7.9) earthquake, *Nature*, *458*(7235), 194–197, doi:10.1038/nature07837.

Jiang, M., A. Galvé, A. Hirn, B. de Voogd, M. Laigle, H. P. Su, J. Diaz, J. C. Lepine, and Y. X. Wang (2006), Crustal thickening and variations in architecture from the Qaidam basin to the Qang Tang (north-central Tibetan Plateau) from wide-angle reflection seismology, *Tectonophysics*, *412*(3–4), 121–140, doi:10.1016/j.tecto.2005.09.011.

Kao, H., R. Gao, R. J. Rau, D. N. Shi, R. Y. Chen, Y. Guan, and F. T. Wu (2001), Seismic image of the Tarim basin and its collision with Tibet, *Geology*, *29*(7), 575–578, doi:10.1130/0091-7613(2001)029<0575:SIOTTB>2.0.CO;2.

Kapp, P., A. Yin, T. M. Harrison, and L. Ding (2005), Cretaceous-Tertiary shortening, basin development, and volcanism in central Tibet, *Geol. Soc. Am. Bull.*, *117*(7–8), 865–878, doi:10.1130/B25595.1.

Kapp, P., P. G. DeCelles, G. E. Gehrels, M. Heizier, and L. Ding (2007), Geological records of the Lhasa-Qiangtang and Indo-Asian collisions in the Nima area of central Tibet, *Geol. Soc. Am. Bull.*, *119*(7–8), 917–933, doi:10.1130/B26033.1.

Karplus, M. S., W. Zhao, S. L. Klemperer, Z. Wu, J. Mechie, D. Shi, L. D. Brown, and C. Chen (2011), Injection of Tibetan crust beneath the south Qaidam basin: Evidence from INDEPTH IV wide-angle seismic data, *J. Geophys. Res.*, *116*, B07301, doi:10.1029/2010JB007911.

Kind, R., et al. (2002), Seismic images of crust and upper mantle beneath Tibet: Evidence for Eurasian plate subduction, *Science*, *298*(5596), 1219–1221.

King, R. W., F. Shen, B. Clark Burchfiel, L. H. Royden, E. Wang, Z. Chen, Y. Liu, X.-Y. Zhang, J.-X. Zhao, and Y. Li (1997), Geodetic measurement of crustal motion in southwest China, *Geology*, *25*(2), 179–182, doi:10.1130/0091-7613(1997)025<0179:GMOCMI>2.3.CO;2.

Klemperer, S. L. (2006), Crustal flow in Tibet: Geophysical evidence for the physical state of Tibetan lithosphere, and inferred patterns of active flow, *Geol. Soc. Spec. Publ.*, *268*, 39–70.

Lease, R. O., D. W. Burbank, G. E. Gehrels, Z. C. Wand, and D. Y. Yuan (2007), Signatures of mountain building: Detrital zircon U\Pb ages from northeastern Tibet, *Geology*, *35*(3), 239–342, doi:10.1130/G23057A.1.

Lease, R. O., D. W. Burbank, M. K. Clark, K. A. Farley, D. Zheng, and H. Zhang (2011), Middle Miocene reorganization of deformation along the northeastern Tibetan Plateau, *Geology*, *39*(4), 359–362, doi:10.1130/G31356.1.

Lease, R. O., D. W. Burbank, B. G. Hough, Z. C. Wang, and D. Y. Yuan (2012), Pulsed Miocene range growth in northeastern Tibet: Insights from Xunhua basin magnetostratigraphy and provenance, *Geol. Soc. Am. Bull.*, *124*(5–6), 657–677, doi:10.1130/B30524.1.

Liu, M. J., W. D. Mooney, S. L. Li, N. Okaya, and S. Detweiler (2006), Crustal structure of the northeastern margin of the Tibetan Plateau from the Songpan-Ganzi terrane to the Ordos basin, *Tectonophysics*, *420*(1–2), 253–266, doi:10.1016/j.tecto.2006.01.025.

Liu-Zeng, J., P. Tapponnier, Y. Gaudemer, and L. Ding (2008), Quantifying landscape differences across the Tibetan Plateau: Implications for topographic relief evolution, *J. Geophys. Res.*, *113*, F04018, doi:10.1029/2007JF000897.

McClay, K. R., and P. G. Buchanan (1992), Thrust faults in inverted extensional basins, in *Thrust Tectonics*, 93–104, Chapman and Hall, London.

Molnar, P., and P. Tapponnier (1981), A possible dependence of tectonic strength on the age of the crust in Asia, *Earth Planet. Sci. Lett.*, *52*(1), 107–114.

Molnar, P., and J. M. Stock (2009), Slowing of India's convergence with Eurasia since 20 Ma and its implications for Tibetan mantle dynamics, *Tectonics*, *28*, TC3001, doi:10.1029/2008TC002271.

Molnar, P., W. R. Boos, and D. S. Battisti (2010), Orographic controls on climate and paleoclimate of Asia: Thermal and mechanical roles for the Tibetan Plateau, *Annu. Rev. Earth Planet. Sci.*, *38*, 77–102, doi:10.1146/annurev-earth-040809-152456.

Murphy, M. A., A. Yin, T. M. Harrison, S. B. Durr, Z. Chen, F. J. Ryerson, W. S. F. Kidd, X. Wang, and X. Zhou (1997), Did the Indo-Asian collision alone create the Tibetan Plateau?, *Geology*, *25*(8), 719–722, doi:10.1130/0091-7613(1997)025<0719:DTIACA>2.3.CO;2.

Nabelek, J., G. Hetenyi, J. Vergne, S. Sapkota, B. Kafle, M. Jiang, H. P. Su, J. Chen, B. S. Huang, and H.-C. Team (2009), Underplating in the Himalaya-Tibet collision zone revealed by the Hi-CLIMB Experiment, *Science*, *325*(5946), 1371–1374, doi:10.1126/science.1167719.

Najman, Y., et al. (2010), Timing of India-Asia collision: Geological, biostratigraphic, and palaeomagnetic constraints, *J. Geophys. Res.*, *115*, B12416, doi:10.1029/2010JB007673.

Oskin, M. E., and D. W. Burbank (2007), Transient landscape evolution of basement-cored uplifts: Example of the Kyrgyz Range, Tian Shan, *J. Geophys. Res.*, *112*, F03S03, doi:10.1029/2006JF000563.

Owens, T. J., and G. Zandt (1997), Implications of crustal property variations for models of Tibetan Plateau evolution, *Nature*, *387*(6628), 37–43, doi:10.1038/387037a0.

Pan, S. Z., and F. L. Niu (2011), Large contrasts in crustal structure and composition between the Ordos Plateau and the NE Tibetan Plateau from receiver function analysis, *Earth Planet. Sci. Lett.*, *303*(3–4), 291–298, doi:10.1016/j.epsl.2011.01.007.

Qinghai Provincial Bureau of Geology and Mineral Resources (1991), *Regional Geology of the Qinghai Province*, 662 pp., Geol. Publ., Beijing.

Qiusheng, L., G. Rui, L. Deyuan, L. Jingwei, F. Jingyi, Z. Zhiying, L. Wen, L. Yingkang, Y. Quanren, and L. Dexing (2002), Tarim underthrust beneath western Kunlun: Evidence from wide-angle seismic sounding, *J. Asian Earth Sci.*, *20*(3), 247–253, doi:10.1016/S1367-9120(01)00057-8.

Reiners, P. W., and M. T. Brandon (2006), Using thermochronology to understand orogenic erosion, *Annu. Rev. Earth Planet. Sci.*, *34*, 419–466, doi:10.1146/annurev.earth.34.031405.125202.

Ritts, B. D., and U. Biffi (2001), Mesozoic northeast Qaidam basin: Response to contractional reactivation of the Qilian Shan, and implications for the extent of Mesozoic intracontinental deformation in central Asia, in *Paleozoic and Mesozoic Tectonic Evolution of Central Asia: From Continental Assembly to Intracontinental Deformation*, 293–316, Geol. Soc. of Am., Boulder, Colo.

Robert, A., J. Zhu, J. Vergne, R. Cattin, L. S. Chan, G. Wittlinger, G. Herquel, J. de Sigoyer, M. Pubellier, and L. D. Zhu (2010), Crustal structures in the area of the 2008 Sichuan earthquake from seismologic and gravimetric data, *Tectonophysics*, *491*(1–4), 205–210, doi:10.1016/j.tecto.2009.11.010.

Rowley, D. B., R. T. Pierrehumbert, and B. S. Currie (2001), A new approach to stable isotope-based paleoaltimetry: Implications for paleoaltimetry and paleohypsometry of the high Himalaya since the late Miocene, *Earth Planet. Sci. Lett.*, *188*(1–2), 253–268, doi:10.1016/S0012-821X(01)00324-7.

Royden, L. H., B. C. Burchfiel, R. W. King, E. Wang, Z. L. Chen, F. Shen, and Y. P. Liu (1997), Surface deformation and lower crustal flow in eastern Tibet, *Science*, *276*(5313), 788–790, doi:10.1126/science.276.5313.788.

Royden, L. H., B. C. Burchfiel, and R. D. van der Hilst (2008), The geological evolution of the Tibetan Plateau, *Science*, *321*(5892), 1054–1058, doi:10.1126/science.1155371.

Seeber, L., and C. C. Sorlien (2000), Listric thrusts in the western transverse ranges, California, *Geol. Soc. Am. Bull.*, *112*(7), 1067–1079, doi:10.1130/0016-7606(2000)112<1067:LTITWT>2.0.CO;2.

Shi, D. N., Y. Shen, W. J. Zhao, and A. B. Li (2009), Seismic evidence for a Moho offset and south-directed thrust at the easternmost Qaidam-Kunlun boundary in the northeast Tibetan Plateau, *Earth Planet. Sci. Lett.*, *288*(1–2), 329–334, doi:10.1016/j.epsl.2009.09.036.

Shuster, D. L., and K. A. Farley (2005), $^{4}He/^{3}He$ thermochronometry: Theory, practice, and potential complications, *Rev. Mineral. Geochem.*, *58*(1), 181–203, doi:10.2138/rmg.2005.58.7.

Suppe, J. (1983), Geometry and kinematics of fault-bend folding, *Am. J. Sci.*, *283*(7), 684–721, doi:10.2475/ajs.283.7.684.

Vincent, S. J., and M. B. Allen (1999), Evolution of the Minle and Chaoshui basins, China: Implications for Mesozoic strike-slip basin formation in Central Asia, *Geol. Soc. Am. Bull.*, *111*(5), 725–742, doi:10.1130/0016-7606(1999)111<0725:EOTMAC>2.3.CO;2.

Wang, C. Y., W. B. Han, J. P. Wu, H. Lou, and W. W. Chan (2007), Crustal structure beneath the eastern margin of the Tibetan Plateau and its tectonic implications, *J. Geophys. Res.*, *112*, B07307, doi:10.1029/2005JB003873.

Wang, C. Y., H. Lou, P. G. Silver, L. P. Zhu, and L. J. Chang (2010a), Crustal structure variation along 30°N in the eastern Tibetan Plateau and its tectonic implications, *Earth Planet. Sci. Lett.*, *289*(3–4), 367–376, doi:10.1016/j.epsl.2009.11.026.

Wang, C. Y., L. P. Zhu, H. Lou, B. S. Huang, Z. X. Yao, and X. H. Luo (2010b), Crustal thicknesses and Poisson's ratios in the eastern Tibetan Plateau and their tectonic implications, *J. Geophys. Res.*, *115*, B11301, doi:10.1029/2010JB007527.

Wang, Z. C., et al. (2012), Magnetostratigraphy and depositional history of the Miocene Wushan basin on the NE Tibetan Plateau, China: Implications for middle Miocene tectonics of the west Qinling fault zone, *J. Asian Earth Sci.*, *44*, 189–202, doi:10.1016/j.jseaes.2011.06.009.

Wittlinger, G., J. Vergne, P. Tapponnier, V. Farra, G. Poupinet, M. Jiang, H. Su, G. Herquel, and A. Paul (2004), Teleseismic imaging of subducting lithosphere and Moho offsets beneath western Tibet, *Earth Planet. Sci. Lett.*, *221*(1–4), 117–130, doi:10.1016/S0012-821X(03)00723-4.

Xu, L. L., S. Rondenay, and R. D. van der Hilst (2007), Structure of the crust beneath the southeastern Tibetan Plateau from teleseismic receiver functions, *Phys. Earth Planet. Inter.*, *165*(3–4), 176–193, doi:10.1016/j.pepi.2007.09.002.

Yin, A., and T. M. Harrison (2000), Geologic evolution of the Himalayan-Tibetan orogen, *Annu. Rev. Earth Planet. Sci.*, *28*, 211–280, doi:10.1146/annurev.earth.28.1.211.

Yin, A., et al. (2002), Tectonic history of the Altyn Tagh fault system in northern Tibet inferred from Cenozoic sedimentation, *Geol. Soc. Am. Bull.*, *114*(10), 1257–1295, doi:10.1130/0016-7606(2002)114<1257:THOTAT>2.0.CO;2.

Yin, A., Y. Dang, M. Zhang, M. W. McRivette, W. P. Burgess, and X. Chen (2007), Cenozoic tectonic evolution of Qaidam basin and its surrounding regions (part 2): Wedge tectonics in southern Qaidam basin and the Eastern Kunlun Range, *Spec. Pap. Geol. Soc. Am.*, *433*, 369–390, doi:10.1130/2007.2433(18).

Yin, A., Y. Q. Dang, L. C. Wang, W. M. Jiang, S. P. Zhou, X. H. Chen, G. E. Gehrels, and M. W. McRivette (2008a), Cenozoic tectonic evolution of Qaidam basin and its surrounding regions (Part 1): The southern Qilian Shan-Nan Shan thrust belt and northern Qaidam basin, *Geol. Soc. Am. Bull.*, *120*(7–8), 813–846, doi:10.1130/B26180.1.

Yin, A., Y. Q. Dang, M. Zhang, X. H. Chen, and M. W. McRivette (2008b), Cenozoic tectonic evolution of the Qaidam basin and its surrounding regions (Part 3): Structural geology, sedimentation, and regional tectonic reconstruction, *Geol. Soc. Am. Bull.*, *120*(7–8), 847–876, doi:10.1130/B26232.1.

Zhang, H., W. H. Craddock, R. O. Lease, W. Wang, D. Y. Yuan, P. Zhang, P. Molnar, D. Zheng, and W. Zheng (2012), Magnetostratigraphy of the Neogene Chaka basin and its implications for mountain building processes in the northeastern Tibetan Plateau, *Basin Res.*, *24*(1), 31–50, doi:10.1111/j.1365-2117.2011.00512.x.

Zhang, P. Z., Z. Shen, M. Wang, W. J. Gan, R. Burgmann, and P. Molnar (2004), Continuous deformation of the Tibetan Plateau from Global Positioning System data, *Geology*, *32*(9), 809–812, doi:10.1130/G20554.1.

Zhao, J. M., W. D. Mooney, X. K. Zhang, Z. C. Li, Z. J. Jin, and N. Okaya (2006), Crustal structure across the Altyn Tagh Range at the northern margin of the Tibetan Plateau and tectonic implications, *Earth Planet. Sci. Lett.*, *241*(3–4), 804–814, doi:10.1016/j.epsl.2005.11.003.

Zhao, W., et al. (2001), Crustal structure of central Tibet as derived from project INDEPTH wide-angle seismic data, *Geophys. J. Int.*, *145*(2), 486–498, doi:10.1046/j.0956-540x.2001.01402.x.

Zheng, D. W., P. Z. Zhang, J. L. Wan, D. Y. Yuan, C. Y. Li, G. M. Yin, G. L. Zhang, Z. C. Wang, W. Min, and J. Chen (2006), Rapid exhumation at ~8 Ma on the Liupan Shan thrust fault from apatite fission-track thermochronology: Implications for growth of the northeastern Tibetan Plateau margin, *Earth Planet. Sci. Lett.*, *248*(1–2), 198–208, doi:10.1016/j.epsl.2006.05.023.

Zheng, D. W., M. K. Clark, P. Zhang, W. Zheng, and K. A. Farley (2010), Erosion, fault initiation and topographic growth of the north Qilian Shan (northern Tibetan Plateau), *Geosphere*, *6*(6), 937–941, doi:10.1130/GES00523.1.

Zheng, W. J., P. Z. Zhang, W. G. He, D. Y. Yuan, Y. X. Shao, D. W. Zheng, W. P. Ge, and W. Min (2012), Transformation of displacement between strike-slip and crustal shortening in the northern margin of the Tibetan Plateau: Evidence from decadal GPS measurements and late Quaternary slip rates on faults, *Tectonophysics*, doi:10.1016/j.tecto.2012.01.006, in press.

Zhu, B., W. S. F. Kidd, D. B. Rowley, B. S. Currie, and N. Shafique (2005), Age of initiation of the India-Asia collision in the east-central Himalaya, *J. Geol.*, *113*(3), 265–285, doi:10.1086/428805.